TriDurLE

National Center for Transportation Infrastructure Durability & Life-Extension

Project ID: 2022-WSU-02

Nanomodified Cementitious Composites Incorporating Waste Polymer Microfibers for Durable and Environmentally Friendly Infrastructure

Final Report

By

PI: Xianming Shi, PhD, F. ASCE, Professor, Washington State University
Co-PI: Zhipeng Li, Postdoc Research Associate, Washington State University

for

National University Transportation Center TriDurLE
Department of Civil & Environmental Engineering
405 Spokane Street PO Box 642910
Washington State University Pullman, WA 99164-2910

Date
10/31/2025

Acknowledgements

The work presented in this report was sponsored by the National Center for Transportation Infrastructure Durability & Life Extension (TriDurLE), and this support is gratefully acknowledged. The authors also wish to express their sincere appreciation to all individuals who contributed to this research. Special thanks are extended to Mr. Jan Benedict B. Mislang, who served as an undergraduate research assistant at Washington State University (WSU) and is now a transportation engineer with the Washington State Department of Transportation; Mr. Venkat Sai Vinay Angara and Ms. Noor Nasser Humaid Aljabri, who also served as undergraduate research assistants at WSU; and Dr. Sailong Hou of WSU for his assistance with SEM investigations. The authors further thank Dr. Meili Liu and Mr. Kingshuk Mukherjee at the University of Miami for their valuable assistance and expertise in microscopic analyses.

Disclaimer

Table of Contents

List of Figures

List of Tables

Executive Summary

This report presents a three-phase research effort aimed at developing and evaluating a sustainable approach for upcycling discarded medical masks and textile waste into high-performance cementitious composites. The primary objective was to apply nanomaterial surface modification techniques, specifically graphene oxide (GO) and nanoclay (NC), to enhance the interfacial bonding, mechanical performance, and durability of ordinary Portland cement (OPC)-based composites while identifying cost-effective alternatives to commercial synthetic fibers.

In the first phase, waste-derived microfibers (WMF) were fabricated from discarded masks and textiles using a high-speed mechanical processing method and subsequently treated with GO or NC. Microstructural characterization confirmed successful nanomaterial deposition on fiber surfaces, resulting in increased surface roughness and the introduction of oxygen-containing functional groups that improved fiber–matrix compatibility.

In the second phase, mechanical and durability performance of WMF-reinforced OPC mortars was systematically evaluated. Incorporation of 0.1 vol.% WMF enhanced splitting tensile strength by approximately 32%, while maintaining comparable compressive strength relative to plain OPC mortar. Surface modification with 0.02 wt.% GO further increased splitting tensile strength by up to 59%, whereas NC modification achieved tensile strength gains of approximately 40%. Durability testing demonstrated substantial improvements in resistance to aggressive environments: chloride migration coefficients were reduced by up to 60% and surface electrical resistivity increased to approximately 25 kΩ·cm in NC-modified mortars, indicating a markedly densified pore structure. Under cyclic freeze–thaw exposure, GO-modified mortars exhibited significantly lower mass and strength loss compared with plain OPC and WMF mortars, while sulfate wetting–drying tests showed 10–15% higher strength retention relative to unmodified fiber-reinforced mixtures after prolonged exposure.

In the final phase, microstructural and spectroscopic analyses (SEM, EDS, BSE, and TGA) revealed that GO promoted the formation of denser calcium silicate hydrate (C–S–H) and calcium-rich hydration products, reduced portlandite content, and strengthened the interfacial transition zone. Probabilistic service-life modeling using Weibull distributions indicated that plain OPC mortar could withstand approximately 209 freeze–thaw cycles (≈30 years), whereas WMF-OPC and GO-WMF-OPC mortars could endure approximately 246 cycles (≈35 years) and 256 cycles (≈38 years), respectively.

Overall, the results demonstrate that waste-derived and nanomodified fibers can deliver 30–60% improvements in tensile performance, up to 60% reductions in chloride permeability, and service-life extensions of 5–8 years under freeze–thaw conditions. This study establishes a scalable and environmentally responsible pathway for converting polymeric waste into durable, high-performance cementitious materials suitable for sustainable infrastructure applications.

Chapter 1. Introduction

1.1 Problem Statement

The continuous accumulation of polymeric waste, particularly single-use nonwoven materials and discarded textiles, has become a major environmental concern worldwide. These wastes are primarily composed of polypropylene (PP) and polyester fibers, which possess excellent chemical stability but very limited biodegradability. When disposed of in landfills or released into the environment, they can persist in soils and aquatic systems for decades, gradually fragmenting into microplastics that threaten ecosystems and public health. Conventional disposal methods, such as incineration, are energy-intensive and may release toxic gases and particulate matter. Therefore, it is imperative to develop safe, sustainable, and high-value recycling strategies to convert polymeric waste into functional materials.

Meanwhile, with the ongoing revival of infrastructure investment in the United States, a substantial demand for construction materials is anticipated for new projects and infrastructure rehabilitation. Among these materials, fiber-reinforced cementitious composites constitute a significant portion due to their superior strength, crack resistance, and durability. Polypropylene microfibers (PP fibers) have long been widely used in cementitious composites to control shrinkage cracking, enhance tensile strength, and improve fracture toughness. The fibers bridge microcracks, redistribute stresses, and delay crack propagation, effectively reducing the risk of brittle failure. However, commercial PP fibers are produced primarily from petrochemical feedstocks, which are costly and consume substantial nonrenewable resources. Consequently, converting waste polymers into reinforcing materials for concrete has emerged as a promising approach that reconciles environmental protection with engineering performance.

From both environmental and industrial perspectives, upcycling polymeric and textile waste into recycled PP microfibers offers dual benefits: reducing the ecological burden of persistent plastics and partially substituting commercial synthetic fibers to enhance resource efficiency. According to the U.S. Environmental Protection Agency (EPA), more than 16 million tons of textile waste are generated annually in the United States, with less than 20% being recycled. Even partial utilization of this waste stream in cementitious composites could significantly reduce landfill loads and support circular economy practices in the construction sector. Furthermore, the global market for PP fibers used in construction exceeds $360 million annually, indicating considerable potential for technological adoption and scaling.

Nevertheless, the direct incorporation of waste-derived polymers into cementitious systems presents several scientific and engineering challenges:

First, there is the issue of fiber fabrication and uniformity. Waste polymers and textiles vary in thickness, structure, and composition, making it difficult to process them into microfibers with consistent geometry and surface morphology. Poor control of fiber length or dispersion can lead to agglomeration or localized voids, diminishing composite homogeneity

and strength.

Second, the interfacial transition zone (ITZ) between PP fibers and the cementitious matrix is typically weak due to the hydrophobic and chemically inert nature of PP. Insufficient wetting and adhesion can create microvoids or debonded regions, which act as initiation sites for cracks and fluid penetration. Surface impurities and residual coatings from waste polymers may further exacerbate these compatibility issues. Thus, improving fiber–matrix bonding through surface modification and chemical functionalization remains a central research focus.

Third, the long-term durability of fiber-reinforced composites under realistic service conditions remains insufficiently understood. Concrete structures are often subjected to aggressive environments such as chloride ingress, sulfate attack, and freeze–thaw cycling. Unmodified PP fibers may increase porosity and reduce impermeability, while properly treated fibers can bridge microcracks and enhance resistance to cracking and frost damage. Therefore, understanding the balance between microdefect formation and reinforcement enhancement is essential to optimize the durability of waste-fiber-reinforced composites.

Nanomaterial-assisted interfacial engineering has recently emerged as a practical and scalable strategy to overcome the weak hydrophobic interface of polymer fibers and achieve substantial performance gains with minimal additive dosage. This approach directly supports TriDurLE's mission to advance the durability and reliability of infrastructure through innovative materials and technologies. Although still in the experimental validation stage, accumulated research evidence provides a solid foundation for subsequent performance evaluation, durability prediction, and large-scale implementation.

1.2 Objectives

This research aims to develop a technically feasible and environmentally responsible approach to transform discarded polymeric waste (e.g., masks and textiles) into functional reinforcing fibers for cementitious composites. Building upon previous studies conducted at Washington State University (WSU) and the National Center for Transportation Infrastructure Durability & Life Extension (TriDurLE), this project focuses on addressing the material compatibility, interfacial bonding, and durability performance of waste-derived polypropylene fibers and their nanomodified counterparts.

The specific objectives of this study are as follows:

1. Fabricate and characterize waste-derived fibers: Develop a practical mechanical processing route to convert discarded masks and textiles into polypropylene-based microfibers suitable for cementitious composites, and characterize their geometry, dispersion, and morphology using optical and electron microscopy.
2. Improve interfacial compatibility through nanomaterial modification: Apply graphene oxide (GO) and nanoclay (NC) as surface treatment agents to enhance fiber–matrix bonding. Characterize the modified fiber surfaces in terms of hydrophilicity, roughness, and chemical functionality to verify the effectiveness of nanomaterial-assisted interfacial enhancement.

3. Evaluate mechanical properties of modified composites: Prepare ordinary Portland cement (OPC) mortars incorporating untreated and nanomodified waste fibers and determine their compressive and splitting tensile strengths to assess reinforcement efficiency and fiber–matrix interaction.

4. Assess durability and microstructural performance: Conduct durability tests including chloride migration, freeze–thaw (F/T), and sulfate wetting–drying (W/D) cycles to evaluate long-term resistance to environmental degradation. Perform microstructural and spectroscopic analyses (SEM, BSE, EDS, and TGA) to elucidate the mechanisms by which GO and NC enhance matrix densification and crack resistance.

5. Correlate performance with microstructural mechanisms and service life modeling: Establish correlations between mechanical/durability properties and microstructural evolution to identify key strengthening mechanisms. Apply Weibull-based service-life modeling to predict the number of F/T cycles corresponding to realistic service durations and provide guidance for future scale-up and application of waste-derived, nanomodified fiber composites in sustainable infrastructure.

1.3 Expected Contributions

This research is expected to advance the development of sustainable and durable cementitious composites by establishing an environmentally responsible approach for transforming discarded polymeric masks and textile waste into functional reinforcing fibers. The anticipated scientific and engineering contributions are summarized as follows:

1. Establishing a practical waste-to-resource pathway: The study is expected to demonstrate a feasible and scalable process to convert polymeric mask and textile waste into polypropylene-based microfibers with stable geometry and sufficient dispersion suitable for cementitious applications, providing a foundation for sustainable waste valorization.

2. Demonstrating nanomaterial-assisted interfacial enhancement: By employing graphene oxide (GO) and nanoclay (NC) as surface modifiers, the research will explore how nanomaterial-assisted interfacial engineering can improve fiber–matrix adhesion and interfacial transition zone (ITZ) integrity. The findings are anticipated to confirm enhanced fiber hydrophilicity, roughness, and interfacial bonding performance.

3. Quantifying improvements in mechanical and durability performance: The project is expected to demonstrate that the incorporation of nanomodified waste-derived fibers can significantly enhance the mechanical and durability performance of cementitious composites—specifically tensile strength, crack resistance, and resistance to chloride ingress, freeze–thaw cycling, and sulfate wetting–drying exposure.

4. Establishing structure–performance correlations and service-life prediction: Through microstructural and thermal characterization (SEM, BSE, EDS, and TGA) combined with Weibull-based service-life modeling, the study aims to establish correlations between microstructural modification, matrix densification, and durability enhancement, offering predictive insights for long-term performance under real-world service conditions.

5. Support for TriDurLE's research mission: The expected outcomes will contribute to TriDurLE's mission to enhance the durability, resilience, and sustainability of transportation infrastructure through the adoption of innovative and eco-efficient materials. This research is anticipated to provide a transferable framework for integrating recycled polymer fibers and nanomaterials into next-generation construction composites.

1.4 Report Overview

This report is organized into five main chapters to present the research background, experimental methodology, key findings, and engineering implications in a logical and systematic manner. Chapter 1 introduces the research background and motivation, outlines the challenges associated with incorporating waste-derived polymeric and textile fibers into cementitious composites, and defines the research objectives and expected contributions. Chapter 2 provides a comprehensive review of relevant literature on fiber-reinforced cementitious composites, surface modification techniques, and nanomaterial-assisted interfacial engineering, establishing the scientific and technological context for this study. Chapter 3 details the materials, mixture design, experimental procedures, and analytical methods used for the fabrication, modification, and characterization of waste-derived fibers and their corresponding cementitious composites. Chapter 4 presents and discusses the experimental results, including mechanical performance, microstructural analyses, and durability evaluations under various environmental exposures. The chapter also interprets the mechanistic roles of nanomodified fibers and establishes correlations between microstructure and macroscopic behavior. Chapter 5 concludes the report by summarizing the key findings, highlighting their practical implications for sustainable infrastructure, and providing recommendations for future research and potential field implementation.

Chapter 2. Literature Review

The growing accumulation of polymeric waste has become a serious global environmental challenge (Cui et al., 2023; Skrzyniarz et al., 2022). A significant portion of this waste arises from single-use nonwoven materials and textile products, which are predominantly composed of polypropylene (PP) and polyester. These polymers exhibit high chemical stability and exceptional mechanical performance but are extremely resistant to degradation (De-la-Torre et al., 2023; Lyu et al., 2024). When discarded, they persist in terrestrial and aquatic environments for decades, gradually fragmenting into microplastics that are transported through air and water systems, posing potential ecological and human health risks (Liang et al., 2022; Ray et al., 2022). According to the U.S. Environmental Protection Agency (EPA), over 16 million tons of textile waste are generated each year in the United States, with less than 20% being recycled or reused (Chowdhury et al., 2022). The remaining waste is mostly landfilled or incinerated, contributing to long-term carbon emissions and environmental pollution. Similarly, the surge of single-use polypropylene-based products has intensified plastic waste pressure worldwide. In many regions, nonwoven polymeric materials have become one of the fastest-growing solid waste streams due to their short service life and poor recyclability.

Traditional disposal methods such as landfilling and incineration are increasingly viewed as unsustainable. Landfills require vast areas and may cause soil and groundwater contamination through leachate, while incineration consumes significant energy and releases harmful gases and particulate matter (Lyu et al., 2023; Moazzem et al., 2021). Consequently, the low utilization rate of polymeric and textile wastes underscores an urgent need for high-value recycling and circular economy solutions that transform these persistent materials into functional resources rather than environmental liabilities.

Recent studies have demonstrated that incorporating recycled polymer fibers, particularly those derived from waste masks and textiles, into cementitious composites represents a promising route for waste valorization (Amin et al., 2024; F. Zhang et al., 2024). Polypropylene (PP) fibers obtained from these wastes possess excellent tensile strength, low density, and thermal stability, making them suitable for use as micro-reinforcement in concrete. When appropriately processed, such fibers can reduce plastic waste accumulation while enhancing the performance of cement-based materials. Zhang et al. reported that recycled mask fibers increased the tensile strain capacity of high-strength engineered cementitious composites by up to 2.6%, while mitigating explosive spalling under elevated temperatures by forming vapor release channels as fibers melted (Zhang et al., 2024). Similarly, Wang et al. found that adding 0–4% recycled mask fibers in concrete decreased thermal conductivity by 44.6%, improving thermal insulation and internal stress distribution (Wang et al., 2025). These findings demonstrate that waste mask fibers not only provide mechanical reinforcement but also functional benefits such as energy efficiency and improved durability. Beyond waste masks, recycled textile fibers (e.g., polyester and cotton blends) have also been incorporated into mortar and concrete as secondary reinforcement. Studies indicate that fiber inclusion enhances flexural and impact strength, reduces crack width, and delays failure under load (Friese et al., 2022; Williams Portal et al., 2015). These efforts collectively support a sustainable pathway for

diverting polymeric waste from landfills and reintroducing it into the construction materials cycle.

Despite these advantages, directly incorporating untreated waste-derived fibers into cementitious composites poses several challenges. Polypropylene-based fibers are hydrophobic and chemically inert, leading to weak interfacial bonding with the hydrophilic cement matrix. Poor adhesion may cause microvoids and debonded zones around fibers, which act as crack initiation sites and pathways for fluid ingress, thereby reducing overall strength and durability (Gong et al., 2019; Li et al., 2022). Fiber geometry and dispersion also critically influence mechanical performance. Waste-derived fibers vary in thickness and length depending on their source and processing method. Inconsistent aspect ratios can lead to fiber agglomeration, local heterogeneity, and reduced reinforcement efficiency. Moreover, surface impurities and residual organic coatings from waste textiles may further deteriorate the fiber–matrix interface. To overcome these limitations, recent research has explored surface modification and nanomaterial-assisted interfacial engineering as effective strategies to improve fiber compatibility and interfacial transition zone (ITZ) integrity (Li et al., 2024, 2022).

Graphene oxide (GO) and nanoclay (NC) have emerged as promising surface modifiers due to their abundant functional groups and high surface activity. GO, in particular, contains oxygenated functional groups that enhance fiber hydrophilicity and chemical reactivity. Li et al. demonstrated that GO pretreatment of waste medical mask microfibers significantly improved their bonding with the cement matrix, increasing splitting tensile strength by nearly 47% compared with untreated fibers (Li et al., 2022). Microscopic and spectroscopic analyses revealed that GO promoted the formation of dense calcium–silicate–hydrate (C–S–H) gels, refined pore structure, and reduced portlandite content. Similarly, nanoclay modification has shown the ability to improve interfacial adhesion by providing mechanical interlocking and hydrogen bonding at the fiber surface (Gong et al., 2019). The incorporation of GO or NC into fiber-reinforced mortars not only strengthens the ITZ but also accelerates hydration kinetics, yielding composites with improved mechanical and durability performance. These nanomaterials also serve as crack-bridging agents at the nanoscale, mitigating microcrack propagation under thermal or environmental stresses.

Durability is a critical criterion for the structural application of waste-fiber-reinforced composites. Exposure to freeze–thaw (F/T) cycles and sulfate wet–dry (W/D) conditions often induces cracking, scaling, and loss of mechanical integrity in concrete. Studies show that waste-derived and nanomodified fibers markedly enhance resistance to such deterioration. Li et al. found that GO-pretreated mask fibers improved chloride migration resistance by approximately 50% and enhanced F/T resistance by 20% relative to unmodified composites (Li et al., 2024). The GO coating increased interfacial tortuosity, reduced permeability, and delayed frost-induced microcracking. Lu et al. further reported that hybrid basalt–polyester fiber systems reduced sulfate crystallization and restrained internal expansion, improving compressive and tensile strength retention by more than 40% after 50 W/D cycles (Lu et al., 2025). The combined "surface shielding–internal toughening" mechanism limited ettringite formation and minimized microstructural degradation.

These findings confirm that fiber reinforcement, particularly when combined with nanomaterial surface treatments, can effectively mitigate durability issues associated with aggressive environmental exposures. However, comprehensive studies linking fiber morphology, dispersion uniformity, and long-term degradation kinetics are still limited. Although significant advances have been made in recycling polymeric waste into functional construction materials, several research gaps remain:

1. Limited Recycling Utilization: Global recycling rates for polymeric and textile wastes remain below 20%, leaving vast quantities unvalorized. Large-scale implementation in construction materials could dramatically reduce landfill burdens and carbon emissions.
2. Inadequate Interfacial Characterization: Most existing studies focus on macroscopic strength enhancement, while nanoscale interfacial mechanisms, particularly the interactions between GO or NC and C–S–H phases, require further clarification.
3. Insufficient Long-Term Durability Data: The combined effects of freeze–thaw, sulfate attack, and chloride ingress have rarely been studied under coupled environmental conditions.
4. Scalability and Standardization Issues: Processing consistency, fiber geometry control, and cost-performance balance are key challenges for industrial adoption.
5. Lack of Predictive Modeling and LCA Integration: Life-cycle assessment (LCA) and service-life prediction frameworks are needed to evaluate the true environmental and economic viability of waste-derived fiber composites.

Addressing these gaps will not only promote circular material utilization but also enhance the resilience and sustainability of concrete infrastructure. In particular, nanomaterial-assisted recycling approaches offer a practical route to bridge environmental remediation with advanced materials engineering.

Chapter 3. Methodology

This chapter presents the experimental and analytical methodologies employed to develop, characterize, and evaluate the proposed waste micro-medical mask or textile fiber (WMF)-reinforced cementitious composites and their nanomodified counterparts incorporating graphene oxide (GO) and nanoclay (NC). The overall methodology encompasses the complete workflow, spanning from material processing to performance evaluation, and includes fiber fabrication and surface modification, mortar preparation, mechanical and durability testing, as well as microstructural characterization. Both macro- and micro-scale investigations were conducted to elucidate the reinforcing mechanisms and durability behavior induced by the various nano-treatments and modifications.

3.1 Materials

An ASTM C150 Type I/II ordinary Portland cement (OPC) was used in this study. Its chemical composition, determined by X-ray fluorescence (XRF), is summarized in **Table 0.1**. The fine aggregate was a multipurpose siliceous sand that was prewetted to achieve a saturated surface-dry (SSD) condition prior to proportioning and mixing. The sand, sourced from Bonsal American Inc. (Charlotte, NC), consisted of natural silica with a nominal maximum particle size of 4.75 mm and a fineness modulus of 2.7. The waste masks used were standard three-layer disposable medical masks, which could be easily obtained. Both the waste masks and recycled cotton T-shirts were processed into microfibers using a high-speed blender, as detailed in Section 3.3.

Table 0.1. Chemical composition of OPC (wt. %).

Chemical composition	OPC
SiO_2	20.44
Al_2O_3	3.97
CaO	62.90
Fe_2O_3	4.07
$Na_2O+ K_2O$	0.80
MgO	2.42
SO_3	2.6
Loss on ignition	2.7

Note: Loss on ignition (LOI) was measured by following the ASTM D7348-13: Standard Test Methods for Loss on Ignition (LOI) of solid combustion residues.

The graphene oxide (GO) used in this study was fabricated using a modified Hammer's method, featuring a specific surface area of about 2600 m^2/g and no more than five layers of nanosheet. Based on measurements using an atomic force microscope, the average size of the thickness of the GO was approximately 2 μm and 2 nm, respectively. This GO consisted of about 71 wt.% carbon and 26 wt.% oxygen, and its main functional groups on the surface were O-H, C-H, C-O, C=C, and C=O bonds (**Figure 0.1**), as reported in our previous work (Gong et al., 2024). The nanoclay (NC) used in this project was purchased from Nanocor. Inc. (Hoffman Estates, IL) and had a bulk density of 0.678 g/cm^3 with an aspect ratio of 200 to 400 (Lei et al.,

2021). Based on our previous experience, the dosage of GO/NC was fixed at 0.02% by weight of cement. In addition, the dosage of the polycarboxylate high-range water-reducer (HRWR, MasterGlenium 7920, BASF) was fixed at 0.1 wt. % of cement to guarantee desirable workability.

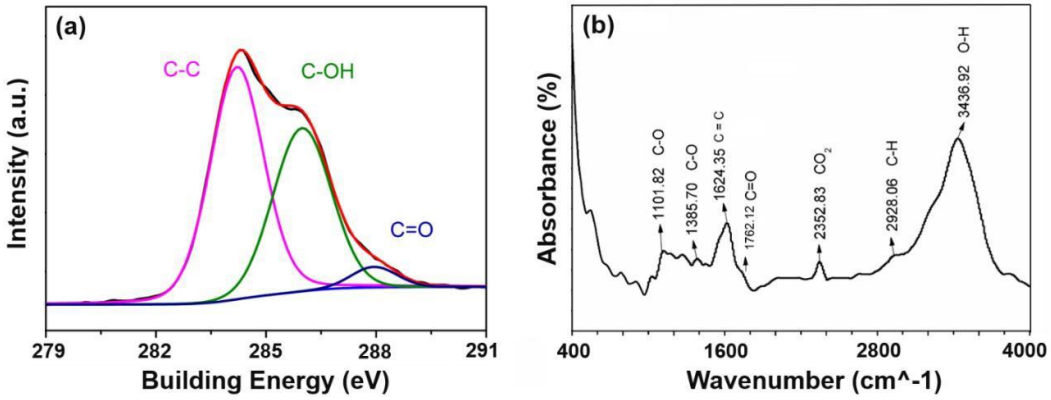

Figure 0.1. (a) XPS and (b) FTIR characterization results of GO used in this study.

3.2 Fabrication of the Specimens

The detailed preparation procedure for WMF is illustrated in **Figure 0.2**, which is also detailed in our previous work (Li et al., 2022). During the preparation process, the mass ratio of shredded masks or textile fibers to water was maintained at 1:10. The blender operated at a rated power of 1000 W and a speed of approximately 30,000 rpm, while the magnetic stirrer was set to about 300 rpm. Since a short duration of 1 minute was sufficient to convert the pieces into single fibers (as shown in **Figure 0.2**), this process was not further optimized.

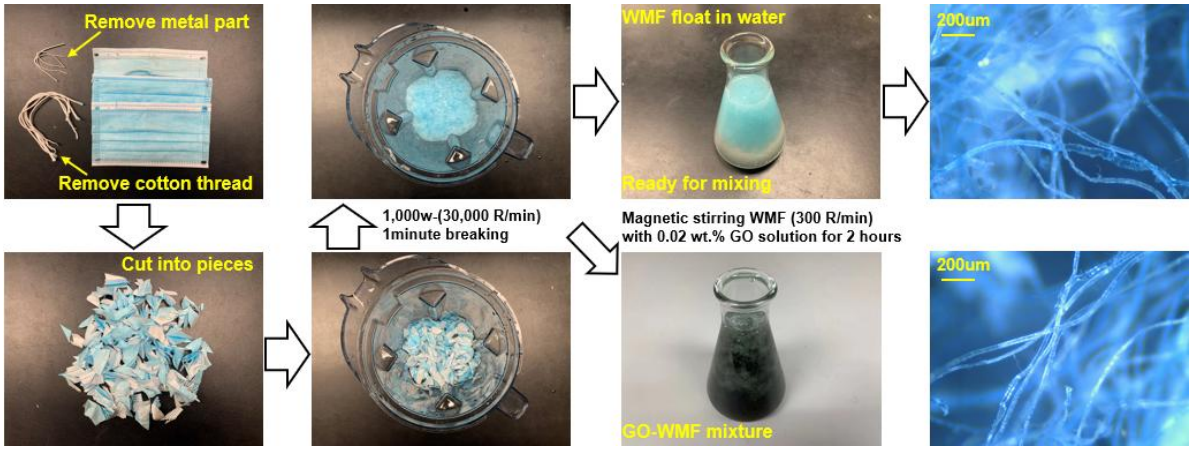

Figure 0.2. Schematic illustration of the fabrication procedure for WMF and GO-WMF fibers.

Two strategies were implemented to incorporate the prepared fibers into the OPC mortar. In the first approach (denoted as F), the fiber suspension was directly mixed with the dry mortar components (cement and fine aggregate). In the second approach (denoted as DF, referring to the inclusion of a drying step), the fibers were first separated from the suspension by filtration while retaining the filtrate. The filtered fibers were then oven-dried to promote stronger bonding between the nanomaterials and the fiber surfaces. Finally, the dried fibers, the retained solution,

and the dry mortar mixture were combined and mixed uniformly. This second strategy was designed to improve the surface treatment efficiency of the WMF and thereby enhance the interfacial transition zone (ITZ) between the fibers and the cementitious matrix.

For the mortar samples incorporating nano-treated fibers, the cement-to-fine aggregate ratio was fixed at 1:3 and the water-to-cement ratio was fixed at 0.4. The volume ratio of fibers to OPC mortar was fixed at 0.1% which corresponds to a mass ratio of about 1 %, and the HRWR was introduced into the pieces-breaking process to facilitate the dispersion of fibers and nanomaterials (GO & NC). The fabrication of nano-treated fibers reinforced OPC mortar samples was carried out in the laboratory following the ASTM C341/C341M-18. After completing the mixing process, the fresh mortar was cast into cylindric molds (D2" × H4") and cured in a standard environment (temperature = 18 °C~22 °C, relative humidity = 95%~98%). After curing for 24 h, the mortar samples were demolded and then cured in the same environment for the designed time before further investigation.

3.3 Mechanical Testing

The compressive strength of cylindrical mortar samples was tested following the ASTM C39/C39M-20. A compressive axial load was applied to cylinders (D2" × H4") until failure occurred. The peak load was recorded to calculate the compressive strength. The splitting tensile strength was tested following the ASTM C496/C496M-17. A compressive load was applied to the side axis of cylinders (D2" × H4") until failure occurred. The peak load was recorded to calculate the splitting tensile strength following the formula proposed by the ASTM C496. For both strengths, three results were averaged as the final reported strength.

3.4 Macroscale Property Evaluation

The non-steady-state chloride migration coefficient of cylindrical mortar samples was performed following the NT Build 492 (a.k.a., rapid chloride migration test: RCM). Each disc sample (D4" × H2") used for this test was cut from the D4" × H8" cylinder after removing the 1" layer on the top/bottom side. After being saturated in saturated $Ca(OH)_2$ aqueous solution, these SSD disc samples were moved to the test machine (**Figure 0.3a**) for chloride migration testing. The catholyte used was 10 wt.% NaCl solution and the anolyte was 0.3 M NaOH solution, respectively. After 24 hours of chloride migration, each disc sample was split and 0.1 M AgNO3 solution was then sprayed on the splitting section as a staining test to trace the penetration depth of chloride. Ten locations at the AgCl-dyed penetration depth were measured, and the non-steady-state chloride migration coefficient DRCM was calculated using the formula (**Equation 3.1**) proposed by the NT Build 492.

$$D_{RCM} = \frac{0.0239(273+T)L}{(U-2)t}\left(X_d - 0.0238\sqrt{\frac{(273+T)LX_d}{U-2}}\right) \quad (3.1)$$

Where T is the average temperature of the original and final solution (°C), L is the thickness of samples (mm), U is the applied voltage (V), t is the duration of testing (h), and Xd is the penetration depth of chloride (mm).

The surface electrical resistivity of cylindrical mortar samples was measured following

the AASHTO TP 95-2014, which also provides an indirect indication of the microstructure and can correlate with the chloride resistance of saturated cementitious materials. After curing for 28 days, the designed mortar cylinders (D4" × H8") were vacuum-soaked in deionized water at room temperature for 24 h to achieve saturation. A four probes-four channels testing device (**Figure 0.3b**) was then employed to measure the surface electrical resistivity of the SSD cylindrical mortar:

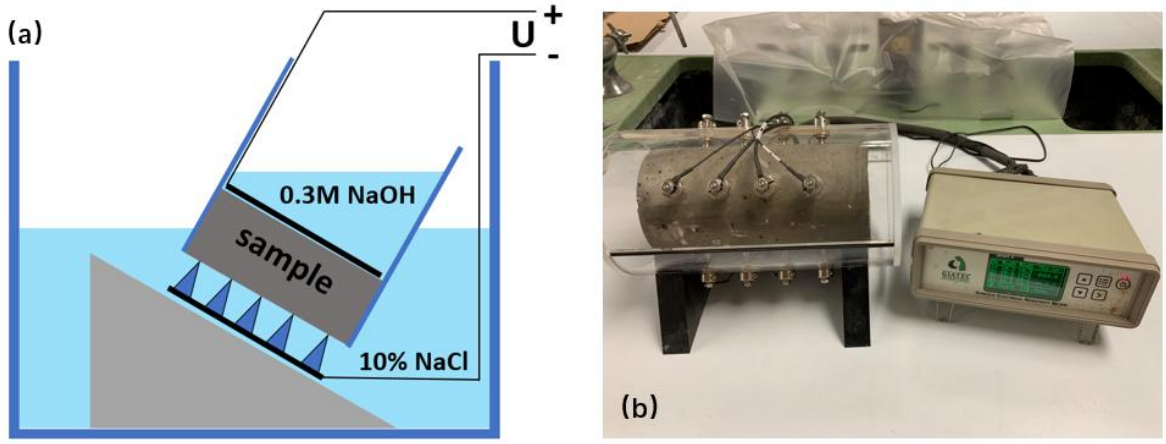

Figure 0.3. Experimental setups for (a) rapid chloride migration testing and (b) surface electrical resistivity measurement (per NT Build 492 and AASHTO TP 95).

The freezing-thawing (F/T) performance of cylindrical mortar samples was evaluated following the ASTM C666. The sample size in this test was D2" × H4", and each F/T cycle took approximately 5.6 hours. Note that the temperature inside the mortar cylinder was not the same as the temperature of the solution immersing the cylinders, which has been reported in our previous work (Lei et al., 2021). After every 12 F/T cycles, the location of each sample was randomly adjusted, and each sample was upside down after every 24 cycles. In addition, deionized water was supplied regularly to guarantee that all samples were effectively immersed. The mass loss and compressive strength loss were recorded periodically to evaluate the F/T resistance of various types of mortar specimens.

The sulfate wetting–drying (W/D) resistance of cylindrical mortar specimens was evaluated following the procedures modified from ASTM D559. The specimen size for this test was D2" × H4", consistent with those used for mechanical and F/T resistance testing. Each specimen was fully immersed in a 5 wt.% Na_2SO_4 solution for 12 hours and subsequently dried in an oven at 80 ± 2°C for 12 hours to complete one W/D cycle. Each full cycle lasted approximately 24 hours, and a total of 150 cycles were conducted to simulate long-term sulfate attack. During the test, the solution concentration was maintained by periodic replacement to ensure constant ionic strength, and deionized water was added as necessary to compensate for evaporation losses. After every 10 cycles, the position of each specimen was randomly rotated to minimize location-dependent effects, and specimens were inverted after every 30 cycles to ensure uniform exposure. The mass loss and compressive strength loss were periodically measured after predetermined intervals (every 30 cycles) to quantify the degradation rate. All tests were conducted at consistent laboratory conditions.

3.5 Microstructural and Chemical Characterization

To elucidate the hydration, interfacial bonding, and microstructural evolution of WMF-reinforced cementitious composites and their GO- and NC-modified counterparts prepared via two treatment strategies, a comprehensive suite of microscopic and spectroscopic characterization techniques was employed. Scanning Electron Microscopy (SEM) equipped with Energy Dispersive X-ray Spectroscopy (EDS) was used to observe the micromorphology of fractured cross-sections and to analyze the elemental distribution within the interfacial transition zone (ITZ) between the cement matrix and fibers. Backscattered Electron (BSE) imaging was further utilized to differentiate hydration products and unhydrated cement phases near fiber surfaces. Thermogravimetric Analysis (TGA) was conducted using a PerkinElmer PYRIS 1 analyzer from 50°C to 800°C at a constant heating rate of 10°C/min to quantify the thermal stability of hydrated products, including bound water loss, decomposition of calcium hydroxide, and formation of calcium carbonate.

These techniques were jointly applied to both control and nanomodified WMF-mortar specimens before and after exposure to environmental durability testing (e.g., chloride ingress, freeze–thaw cycling, and sulfate wetting-drying cycles). The results enabled a detailed comparison of microstructural integrity, hydration degree, and interfacial chemical bonding, thereby providing a mechanistic understanding of how GO and NC modification improve the fiber–matrix compatibility and the overall durability of the composite.

Chapter 4. Results and Discussion

This chapter presents and analyzes the experimental results obtained from the investigation of mortar specimens incorporating WMF and their nanomodified counterparts treated with GO and NC using two different strategies. The results are organized to provide a multiscale understanding of material performance and interfacial mechanisms. At the macro scale, the effects of waste-derived fibers, GO, and NC treatment strategies on the mechanical behavior—including compressive and splitting tensile strength—are evaluated and compared. The subsequent sections examine the durability performance of these composites under chloride penetration, freeze–thaw cycling, and sulfate wetting–drying conditions. At the micro scale, microstructural and physicochemical analyses are presented to elucidate hydration characteristics, the fiber–matrix ITZ, and the enhancement mechanisms associated with nanomaterial modification. The chapter concludes with an integrated discussion linking mechanical, durability, and microstructural results to reveal the reinforcing mechanisms and practical implications of upcycling waste polymers into durable cementitious composites.

4.1 Performance Evaluation of Mortar Samples

4.1.1 Compressive Strength

Figure 0.1 indicates that incorporating 0.1 vol.% WMF and its nanomodified counterparts, namely 0.02 wt.% GO-WMF and 0.02 wt.% NC-WMF prepared using the first approach described in **Section 3.2**, resulted in only minor variations in the compressive strength of OPC mortar (**Figure 0.1a**) while significantly enhancing the splitting tensile strength (**Figure 0.1b**). This observation is consistent with our previous work (Li et al., 2022). For instance, the 0.1 vol.% WMF and 0.02 wt.% GO-0.1 vol.% WMF mixtures reduced the 28-day compressive strength of OPC mortar by approximately 8% and 3%, respectively, while enhancing the 28-day splitting tensile strength by 32% and 59%, respectively. These results were also in accordance with the study by Yao et al., in which the introduction of 0.5 vol.% original or 0.5 vol.%-0.8 mg/ml GO pretreated polyvinyl alcohol microfibers caused slight degradation of compressive strength but obvious enhancement of tensile strength of OPC mortar (Yao et al., 2019). The NC-WMF-incorporated mortar showed compressive strength comparable to the control mortar specimens (within 4%) and moderate tensile strength gains of about 40% at 28 days. A similar trend was observed at 7 days, where all fiber-reinforced mortars showed negligible changes in compressive strength but notable enhancements in tensile strength, with the improvement magnitude being highest for GO-WMF, followed by NC-WMF, and then WMF.

The superior splitting tensile strength performance of GO-WMF can be attributed to the two-dimensional structure and abundant oxygen-containing functional groups of GO, which facilitate the formation of strong interfacial bonding between GO, the fibers, and the cement matrix (Gao et al., 2016; He et al., 2021). This enhanced interfacial adhesion improves load transfer efficiency and crack-bridging capability. In contrast, NC primarily acts as a filler and nucleation agent, refining the pore structure, improving matrix homogeneity, and promoting pozzolanic reactions (Gong et al., 2019; Li et al., 2017). However, its weaker chemical interaction with hydration products and fibers results in a less pronounced improvement in

tensile strength. Therefore, GO provides stronger interfacial reinforcement and contributes to the overall mechanical performance, whereas NC mainly enhances structural densification and dimensional stability, leading to a more noticeable improvement in compressive strength.

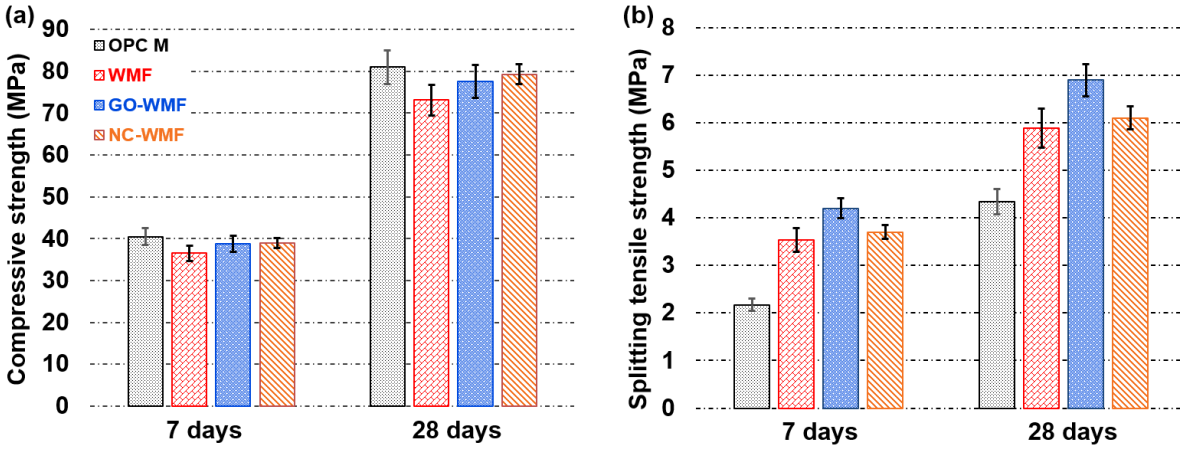

Figure 0.1. (a) compressive strength and (b) splitting tensile strength of OPC mortar incorporating WMF, GO-WMF, and NC-WMF.

Figure 0.2 compares the mechanical performance of mortar specimens incorporating WMF treated with GO and NC using two different approaches. As described in Section 3.2, the "D" series (DGO-WMF and DNC-WMF) involved filtering and drying the nanomodified fibers before mixing, aiming to enhance the interfacial bonding between the fibers and the cementitious matrix. At the macro scale, all mixtures showed comparable compressive strengths, remaining within experimental scatter of each other (**Figure 0.2a**). Both NC-based groups (NC-WMF and DNC-WMF) exhibited slightly higher compressive strength than their GO counterparts, indicating that nanoclay primarily contributed to matrix densification and improved packing efficiency rather than to interfacial reinforcement. In contrast, the splitting tensile strength results (**Figure 0.2b**) reveal a more pronounced effect of the "D" treatment, particularly for the GO system. The DGO-WMF mixture achieved the highest tensile strength, outperforming GO-WMF by roughly 10–15%, confirming that the pre-drying step effectively enhanced fiber–matrix adhesion and stress transfer. For the NC system, a similar trend was observed, with DNC-WMF showing a modest tensile improvement relative to NC-WMF, though the overall enhancement remained less significant than that of the GO series.

The superior splitting tensile strength performance of GO-WMF can be attributed to the two-dimensional structure and abundant oxygen-containing functional groups of GO, which facilitate the formation of strong interfacial bonding between GO, the fibers, and the cement matrix. This enhanced interfacial adhesion improves load transfer efficiency and crack-bridging capability. In contrast, NC primarily acts as a filler and nucleation agent, refining the pore structure, improving matrix homogeneity, and promoting pozzolanic reactions. However, its weaker chemical interaction with hydration products and fibers results in a less pronounced improvement in tensile strength. Therefore, GO provides stronger interfacial reinforcement and contributes to the overall mechanical performance, whereas NC mainly enhances structural densification and dimensional stability, leading to a more noticeable improvement in

compressive strength. The second treatment strategy is more suitable for applications where enhanced tensile performance of cementitious composites is desired. In many practical cases, however, the first treatment strategy performs adequately; thus, the following sections primarily focus on the first strategy.

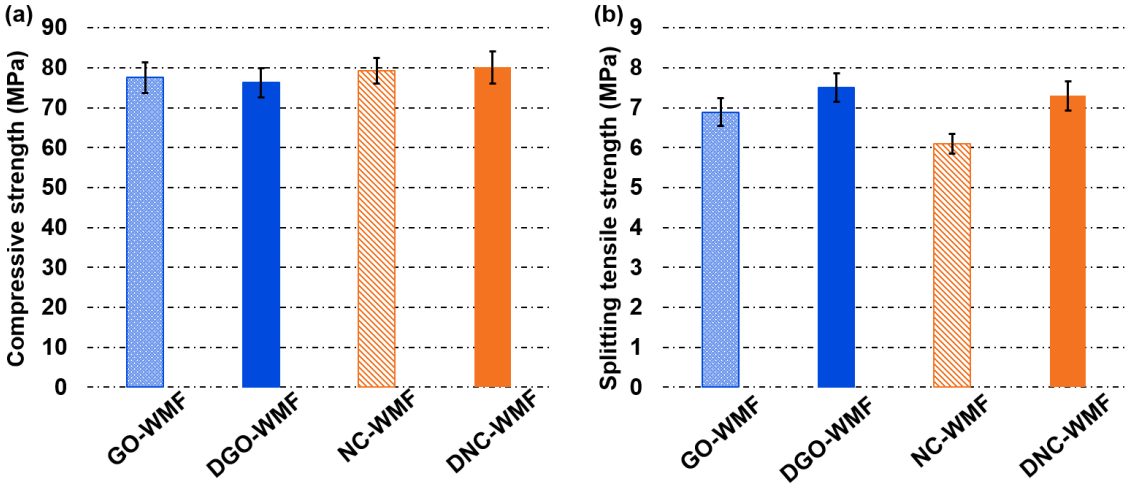

Figure 0.2. (a) compressive strength and (b) splitting tensile strength of mortars incorporating GO-WMF and NC-WMF prepared using different treatment strategies.

4.1.2 Chloride Migration Coefficient and Surface Electrical Resistivity

Figure 0.3 provides the chloride migration depth of one post-RCM mortar sample (**Figure 0.3a**), and the chloride migration coefficient and surface electrical resistivity (**Figure 0.3b**) of all three types of mortar. The admixed WMF increased the chloride migration coefficient of OPC mortar specimen by about 24%, which is likely due to the WMF-introduced microdefects as discussed earlier. These micro-defects resulted in potential channels that facilitate the ingress of chloride anions in the cementitious matrix. The negative effects of fibrous components on the chloride resistance of cementitious material have also been reported in other studies. For instance, Liu et al. demonstrated that admixing too high a dosage of PP fibers compromised the chloride resistance of a concrete because of the higher porosity induced by the fibers (Liu et al., 2019).

Incorporation of nanomaterials effectively mitigated this negative effect. Both GO- and NC-modified mortars exhibited significantly lower chloride migration coefficients and higher surface resistivity values compared with the control and WMF mortars. Among them, the NC-WMF mortar showed the most pronounced improvement, featuring the lowest RCM coefficient (about 60% lower than OPC) and the highest surface electrical resistivity (around 25 kΩ·cm). This superior performance suggests that the layered nanoclay platelets efficiently filled micro-voids and refined the pore network, forming a denser and less permeable microstructure (He and Shi, 2008; Mansi et al., 2022). Additionally, the cation-exchange capacity and pozzolanic reactivity of NC likely enhanced the formation of secondary C–S–H gels, further reducing ionic diffusivity (Li et al., 2017). By comparison, the GO-WMF mortar also achieved notable improvement ($\approx$ 46% reduction in RCM coefficient) owing to the GO-induced densification

of the fiber–matrix ITZ and the increased tortuosity of the chloride transport paths. However, the NC-WMF mixture provided a more continuous and compact matrix, resulting in the highest resistance to chloride penetration. Because the differences between using NC and GO are not significant, and both are sheet-like nanomaterials with similar functions such as negatively charged surfaces, it is reasonable to infer the influence and mechanism of one material based on the experimental investigation of the other. Therefore, the following sections focus on the effects and mechanisms associated with the use of GO.

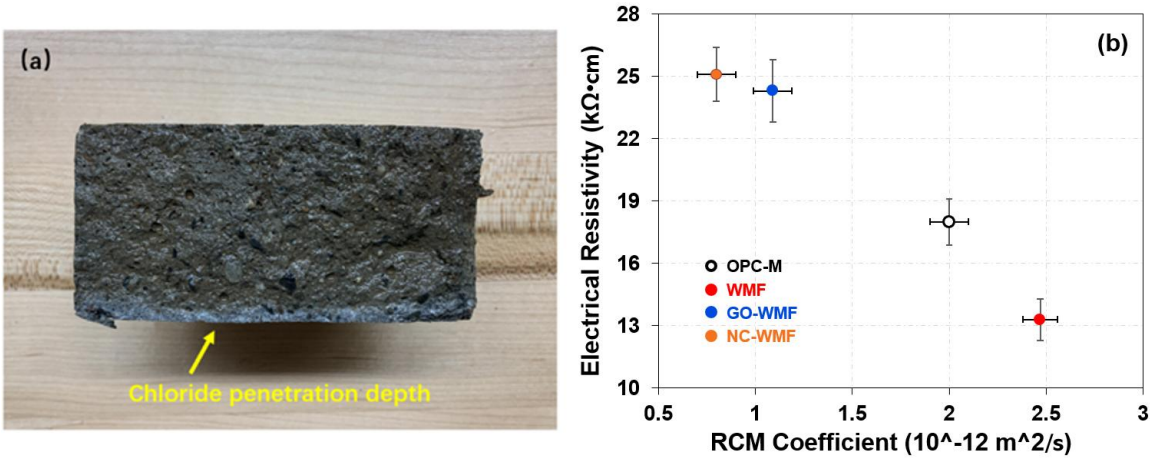

Figure 0.3. (a) chloride penetration depth after rapid chloride migration testing and (b) relationship between surface electrical resistivity and chloride migration coefficient for OPC, WMF, GO-WMF, and NC-WMF mortars (per NT Build 492).

4.2 Durability performance

4.2.1 Cyclic Freeze-Thaw Resistance

With the increase in the number of F/T cycles, there was continued loss of mass and compressive strength of the designed mortar samples, as illustrated in **Figure 0.4.** It is worth noting that the compressive strength of all samples increased slightly at the beginning of the F/T process, which is due to the continued hydration of cement and the leached hydrates filling the micropores. A similar result was reported in another work of ours (Lei et al., 2021).

Compared with the control mortar specimens which almost failed after 210 F/T cycles, the F/T resistance of WMF and GO-WMF mortar specimens was significantly improved. The mass loss of the OPC samples was slow at the beginning during the F/T process but accelerated after approximately 160 cycles, and so did the strength loss. This likely corresponds to how under F/T cycles the microstructure of OPC mortar slowly degrades until significant cracking develops in the mortar matrix along with significant surface scaling. The admixed WWMF, with or without GO pretreatment, enabled the mortar specimens to withstand more F/T cycles. First, the admixed WMF reinforced the mortar and endowed it with better tensile strength, thus slowed down the deterioration of the mortar matrix during the F/T process (Wang et al., 2022). Secondly, the admixed WMF introduced microscopic air bubbles into the mortar matrix, which served as the role played by air-entraining admixtures, i.e., providing the buffering space to mitigate the buildup of tensile stress due to hydraulic, osmotic or ice crystallization pressures

during F/T cycles (Wang et al., 2022). As expected, the admixed GO further improved the F/T resistance of WMF mortar, in terms of less mass loss and higher remaining compressive strength at the same number of F/T cycles. This improvement could be ascribed to the advantageous roles played by GO as mentioned before. The admixed GO not only induced a stronger bond between the WMF and mortar matrix, but also enhanced the mortar matrix because of the free GO in the GO-WMF suspension. Our previous work reported the reduction in water absorption of cementitious materials induced by GO, which also benefits the F/T resistance (He et al., 2018; Li and Shi, 2020). The less the absorbed water, the lower the ice crystallization pressure, and thus the higher the F/T resistance

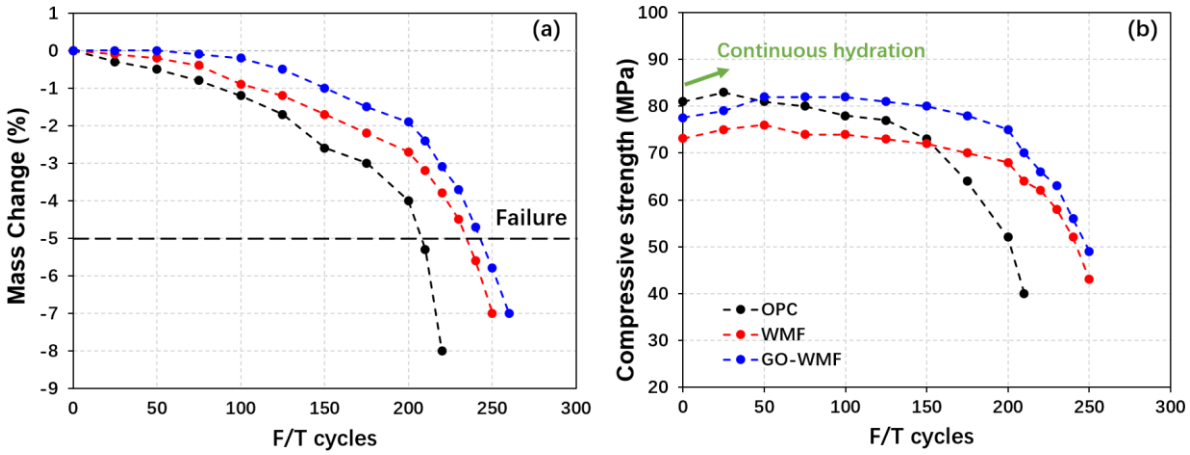

Figure 0.4. (a) mass loss and (b) compressive strength loss of OPC, WMF, and GO-WMF mortar samples subjected to freeze–thaw cycles (per ASTM C666).

Figure 0.5 depicts the microstructure of selected mortar samples to unravel the roles of WMF and GO. As shown in **Figure 0.5a**, the pullout of WMF suggests that the WMF bridged the mortar matrix that was subjected to cracking. The cracks around the embedding end of WMF illustrated the bonding roles played by WMF as well (**Figure 0.5b**), suggesting that the WMF absorbed the fracture energy during the cracking process (Gong et al., 2019; Li et al., 2022). **Figure 0.5c** and **Figure 0.5d** illustrate the microstructure of WMF and GO-WMF mortar specimens after being subjected to cumulative frost damage, respectively. Compared with the evident and wide cracks in WMF mortar, only several narrow cracks (with a maximum crack width of approximately 1 μm) were detected in the GO-WMF mortar. These observations confirm the beneficial role of GO in arresting crack propagation in the WMF mortar matrix and help explain the enhanced mechanical strength and F/T resistance discussed in earlier sections.

4.2.2 Sulfate Resistance under Dry-Wet Cycles

Figure 0.6 illustrates the evolution of compressive and splitting tensile strength of OPC, WMF, and GO-WMF mortars under repeated sulfate wetting–drying (W/D) cycles. A similar degradation trend is observed for all mixtures, where both compressive and tensile strengths gradually decrease with increasing exposure cycles due to the combined effects of sulfate attack, crystal expansion, and microcrack propagation within the matrix.

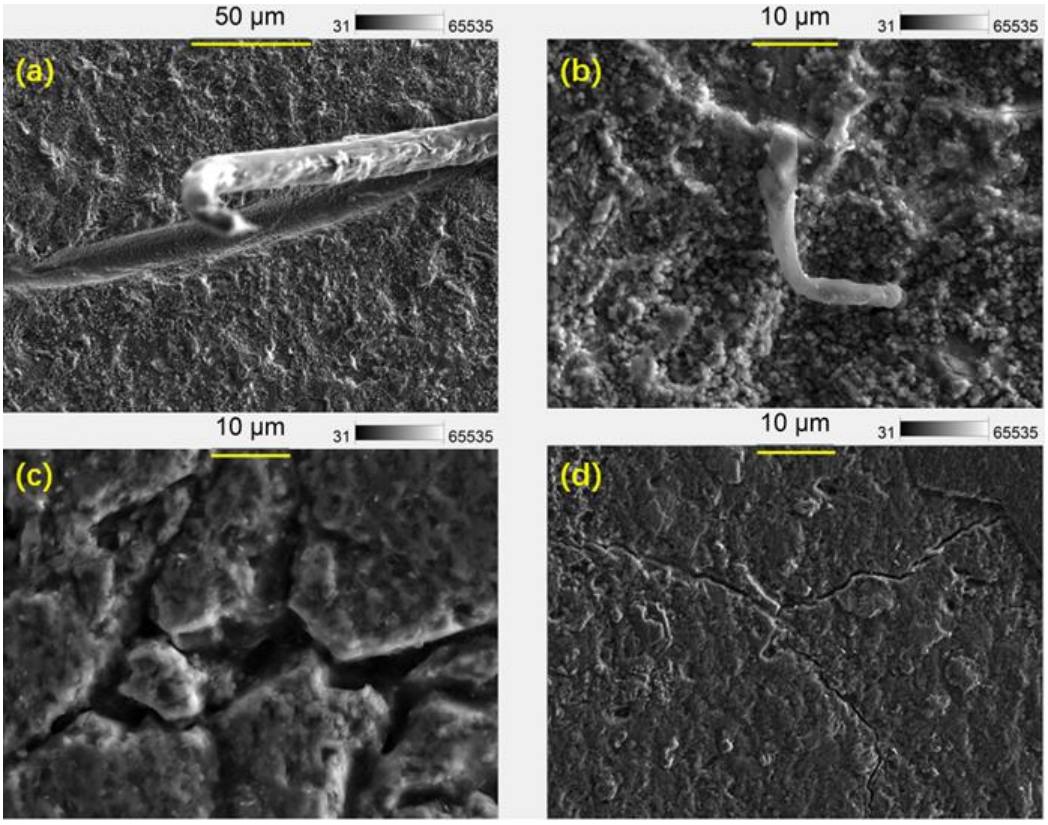

Figure 0.5. Microstructural observations illustrating (a) fiber pullout behavior, (b) pullout-induced cracking around fiber ends, (c) cracks in WMF mortar, and (d) cracks in GO-WMF mortar after freeze–thaw exposure.

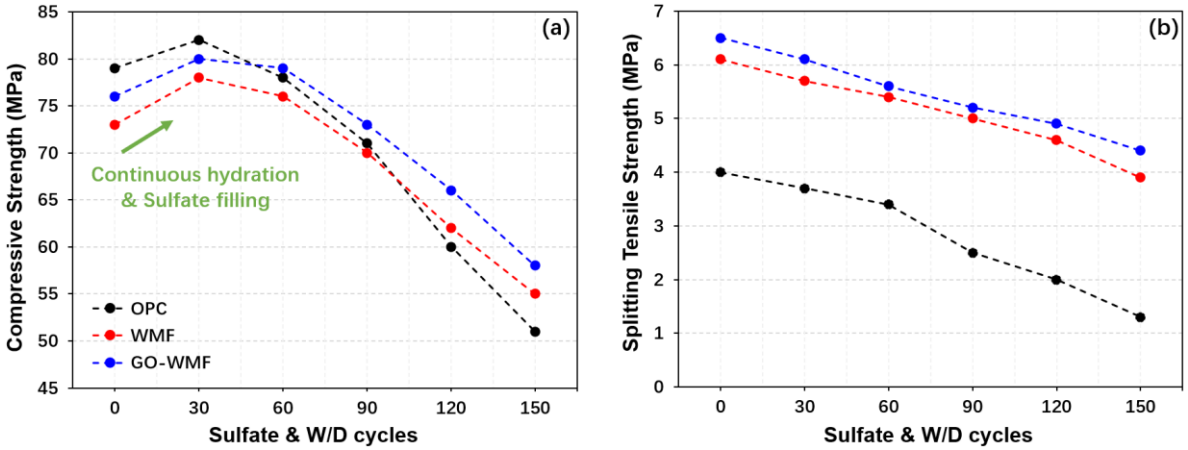

Figure 0.6. (a) compressive strength and (b) splitting tensile strength of OPC, WMF, and GO-WMF mortar samples subjected to sulfate wetting–drying cycles (modified from ASTM D559).

At the early stage (0–30 cycles), all specimens exhibited a slight strength gain, which can be attributed to continued hydration and partial pore filling by sulfate reaction products. After approximately 60 cycles, strength loss became dominant as chemical deterioration and internal stress accumulation outweighed the initial densification benefits. Throughout the entire

exposure period, the WMF and GO-WMF mortars outperformed the OPC mortar samples. The incorporation of WMF effectively reduced microcrack development and delayed sulfate ingress, while the GO-WMF mixture showed the highest resistance to strength degradation. After 150 cycles, the GO-WMF mortar retained approximately 58 MPa in compressive strength and 4.5 MPa in splitting tensile strength, which are roughly 10~15 % higher than those of the WMF mortar and 30~35 % higher than the OPC control. These results demonstrate that the combined effects of GO nanoplatelets and fibrous reinforcement effectively improve sulfate durability. The GO modification enhances the interfacial bonding between fibers and the cementitious matrix and densifies the microstructure, providing improved stress transfer and hindering the diffusion of sulfate ions.

The SEM images and EDS spectra in **Figure 0.7** provide microstructural support for the observed mechanical and durability results. In the WMF mortar (**Figure 0.7a**), the fiber–matrix ITZ exhibits evident sulfate precipitation with acicular or rosette-shaped crystals (inset, **Figure 0.7c**), and the corresponding EDS spectrum (**Figure 0.7b**) shows distinct Sulfate (S) peaks associated with Ca, confirming the formation of gypsum and ettringite. These sulfate-rich deposits are concentrated along the fiber boundary and surrounding microcracks, suggesting that the relatively open ITZ facilitated ionic ingress and crystallization-induced stresses. This observation is consistent with the faster strength deterioration and lower surface resistivity of the WMF mortar during prolonged sulfate wetting–drying cycles.

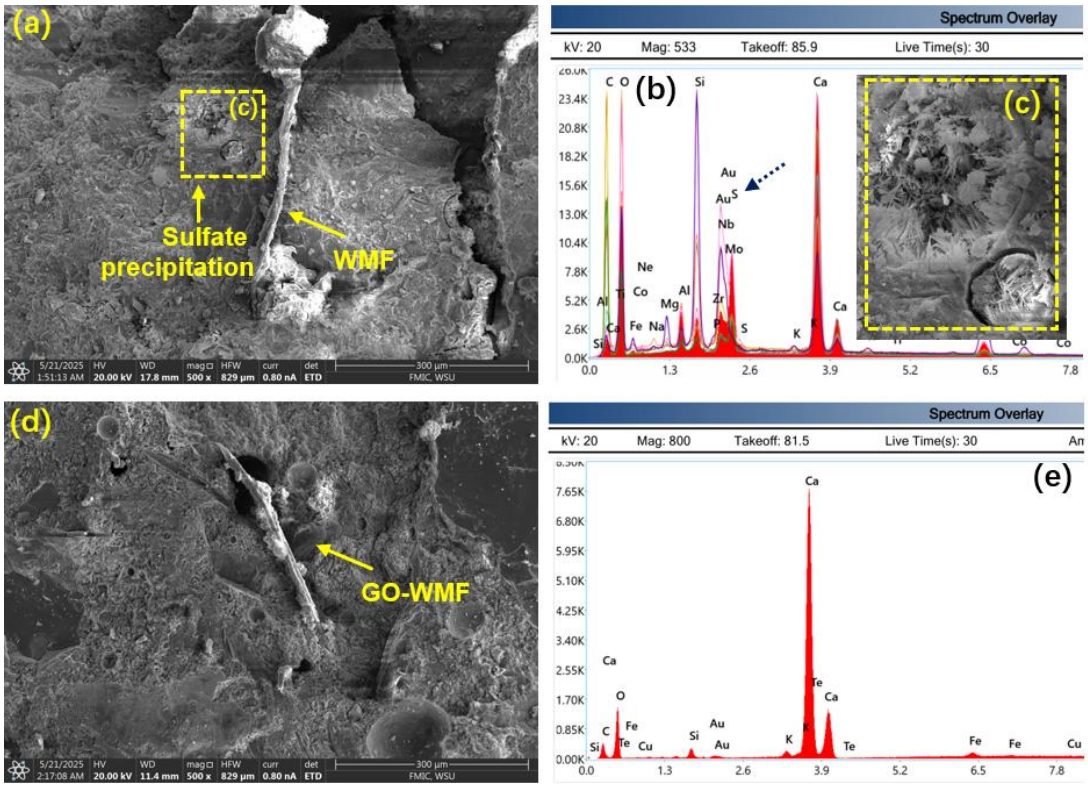

Figure 0.7. (a) SEM of WMF-OPC Mortar, (b) EDS Around the WMF, (c) Sulfate Precipitation in WMF-OPC Mortar, (d) SEM of GO-WMF-OPC Mortar, and (e) EDS Around

the GO-WMF.

In contrast, the GO-WMF mortar (**Figure 0.7d**) exhibits a much denser and more cohesive ITZ, with almost no visible sulfate deposits or microcracks. The EDS spectrum (**Figure 4.7e**) shows negligible S content and a Ca–Si–O–dominated composition, indicating suppressed formation of expansive sulfate products. The absence of visible cracks also reflects a stronger and more intact cementitious matrix, which can be attributed to the matrix-strengthening effect of GO. Numerous previous studies have confirmed that GO promotes hydration reactions and refines pore structure, thereby enhancing the intrinsic strength and compactness of the bulk paste. This strengthened matrix, together with improved fiber–matrix interfacial bonding, significantly limits crack initiation and propagation, reduces sulfate ingress pathways, and ultimately contributes to the superior mechanical and durability performance observed for the GO-WMF mortar.

4.3 Mechanism analysis of improved strength

This section investigates the ITZ performance to elucidate the effects of surface treatment on the fiber–matrix interface, using the GO-WMF mortar as a reference. **Figure 0.8** illustrates the key elemental information collected at the ITZ in WMF-mortar (**Figure 0.8a**) and GO-WMF mortar (**Figure 0.8b**) samples, respectively, which was also reported in our previous work (Li et al., 2022). As shown in **Figure 0.8c**, the negatively charged GO attracts Ca^{2+} to the surface of WMF and repels the $[Al(OH)_4]^{-1}$, which induces the generation of hydrates in higher polymerization degree, as evidenced by the higher Ca/Si and Ca/(Si+Al) mole ratios in **Figure 0.8d**. In addition, the GO nanosheets coated on the surface of WMF not only increased the surface roughness but also facilitated the bond strength between WMF and matrix, this also helps explain the improved mechanical strengths in the GO-WMF mortar composites.

Figure 4.9a and f presents the BSE images of designed paste samples used to determine the hydration degree of OPC in different samples. BSE provides grayscale images which indicate the intensity of a combination of all elements, including H, O, C, Si, Al, Ca, etc. Generally, the darker the grayscale, the lighter the elements (Vespa et al., 2007). In this study, the content of CaO and SiO_2 in the cement used was 62.90 wt.% and 20.44%, respectively, totaling 83.34 wt.%. As such, only Ca and Si elements were considered when analyzing the BSE images. Based on the Ca/Si molar ratios, the hydrates of cement paste could be classified as Si-rich phase (Ca/Si=0~0.67), C-S-H phase (Ca/Si=0.67~2.00), and Ca-rich phase (Ca/Si>2.00) which also contained unhydrated cement particles (Xu et al., 2019). Because no element was detected in the pores and cracks (Ca/Si = 0), we simply incorporated them into the Si-rich phase based on the Ca/Si value. The other reason was that the area content of these pores/cracks counted for only approximately 1% of the total area in this study and thus has insignificant influence on the final analysis. By referencing the related studies (Famy et al., 2002; Xu et al., 2019), the backscatter coefficients of different phases were calculated using Heinrich's empirical equation (Goldstein et al., 2017), and the results are presented in **Table 4.1**. We employed an open-source software ***ImageJ*** software to pre-treat the selected BSE images. Based on the backscatter coefficients, the gray value range of each hydrate phase was

calculated using interpolation between the maximum peak (unhydrated cement in Ca-rich phase) and the minimum peak (pores/cracks/Si-rich phase) of the gray value.

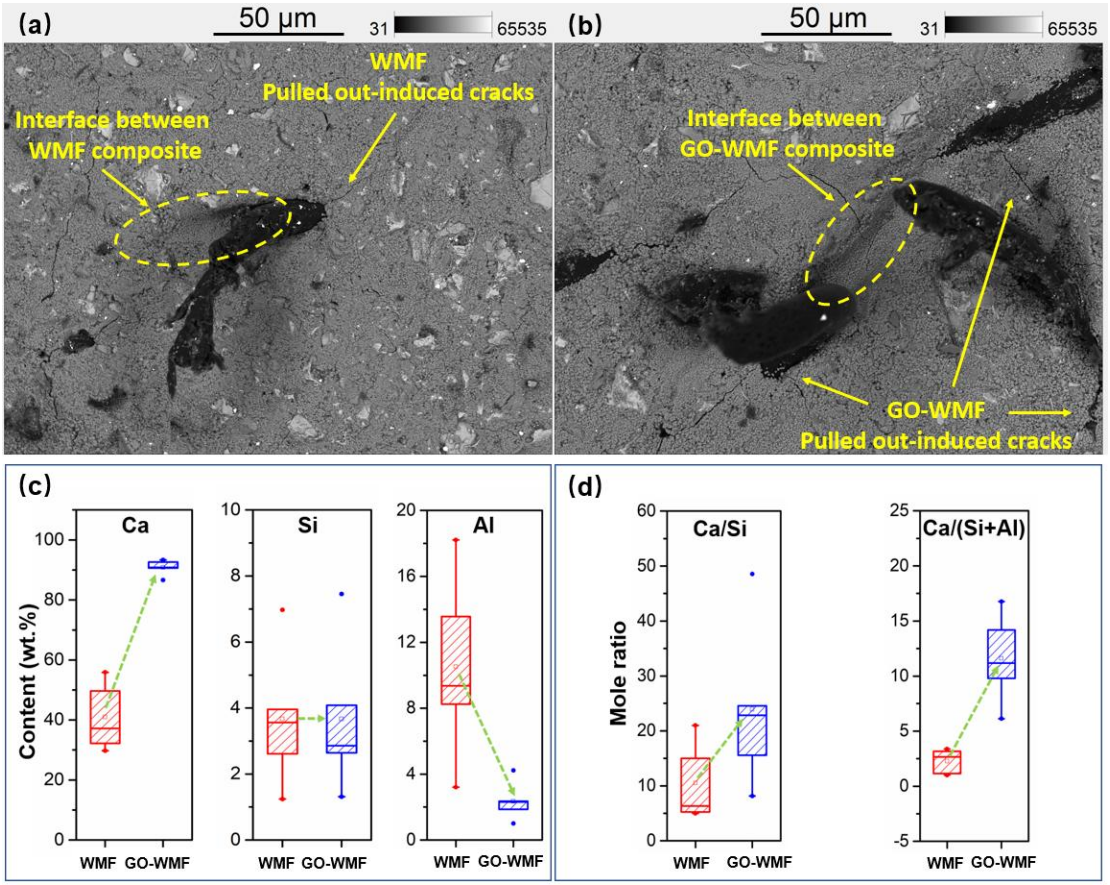

Figure 0.8. Representative BSE of selected (a) WMF-OPC composite; (b) GO-WMF-OPC composite. The (c) content of Ca, Si, and Al; and (d) mole ratio of Ca/Si and Ca/(Si + Al) in WMF vs. GO-WMF composites.

Table 0.1. Area percentage of different hydration phases in selected hardened paste samples at the age of 28 days.

	Hydration Products			
	Si-Rich	C-S-H	Ca-Rich	Unhydrated Cement
BSE Coefficient	0.125-0.142	0.142-0.154	0.154-0.162	0.162-0.186
WMF-OPC	2.44%	48.29%	40.36%	8.91%
GO-WMF-OPC	3.01%	45.12%	45.85%	6.02%
GO's effect	+0.57%	-3.17%	+5.49%	-2.89%

Figure 0.9 provides the segmented patterns of each phase and **Table 0.1** summarizes the area of each individual hydrate phase. **Table 0.1** suggests that the admixed GO increased the amount of Si-rich hydrates (+0.57%) and Ca-rich hydrates (+5.49%), but decreased the amount of C-S-H gel (-3.17%) and unhydrated cement particles (-2.89%). In other words, GO played beneficial roles in accelerating the hydration process and regulating the hydrates of cement. Xu et al. reported a similar effect of admixing GO on the hydrates of OPC paste (Xu et al., 2019).

Our previous work demonstrated an increase of Ca/Si in OPC paste samples due to the incorporation of GO, which is also consistent with this conclusion (Li et al., 2022).

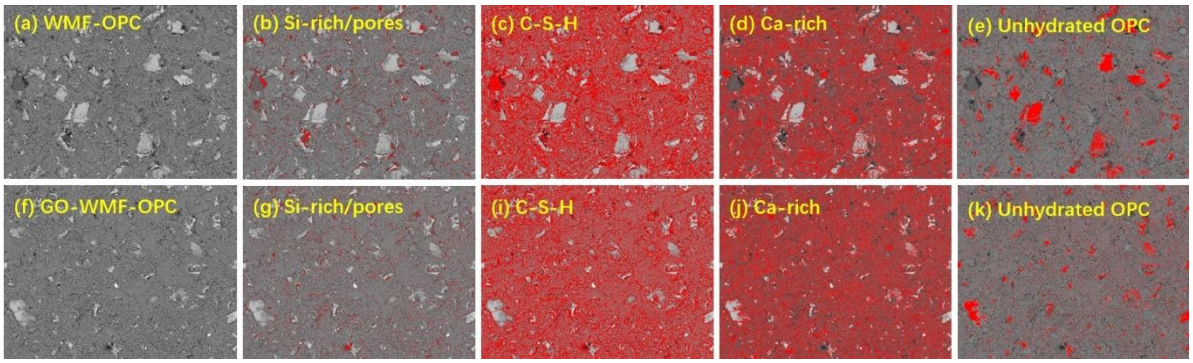

Figure 0.9. (a) WMF-OPC BSE image and its segmented phases: (b) Si-rich/pores, (c) C-S-H, (d) Ca-rich, and (e) unhydrated OPC; (f) GO-WMF-OPC BSE image and its segmented phases: (g) Si-rich/pores, (i) C-S-H, (j) Ca-rich, and (k) unhydrated OPC.

Figure 0.10 depicts the TGA/DTG results of the sampled WMF, OPC, WMF-OPC, and GO-WMF-OPC pastes, which shed light on the changes in their chemical compositions. As shown in **Figure 0.10a**, the degradation of mask microfibers initiated at around 400°C, confirming that their main chemical component was polypropylene; this result also helped to explain the mass loss observed in the WMF and GO-WMF paste samples in the range from 400°C to 500°C (see **Figure 0.10b**). For all the paste samples, the first band of mass loss observed at around 50°C to 180°C can be attributed to the dehydration of C-S-H gel and the decomposition of AFt and AFm (Li and Shi, 2020; Xu et al., 2018).

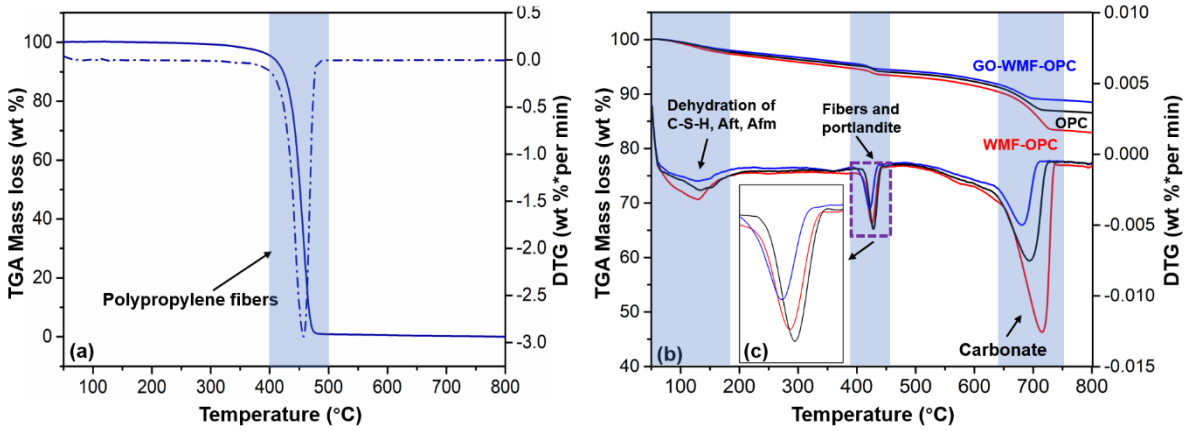

Figure 0.10. (a) TGA/DTG Result of Polypropylene WMF; (b) and (c) TGA/DTG Result of the OPC, WMF, and GO-WMF Paste Samples.

The second obvious band of mass loss was detected at around 400°C to 450°C, corresponding to the decomposition of portlandite and fibers. It is worth noting that the DTG degradation peak (390°C~450°C) of OPC was almost symmetric, indicating only portlandite degraded in this temperature range. However, the peaks detected in WMF-OPC and GO-WMF-OPC were unsymmetric (**Figure 0.10c**), suggesting that portlandite and fibers were decomposed simultaneously in this temperature range. Two Gaussian peaks were thus fitted to

separate the degradation peaks of portlandite and fibers for further quantitative analysis (**Figure 4.11**). After integrating the area under the peak, the mass of portlandite vs. fibers was calculated, and the results are provided in **Figure 4.11** as well. The mass of fibers in WMF-OPC and GO-WMF-OPC was estimated to be 1.20 wt. % and 1.14 wt. %, respectively, which was very close to the designed mass content of about 1.00 wt.%. This result also verified the suitability of the Gaussian peak fitting method used in this study.

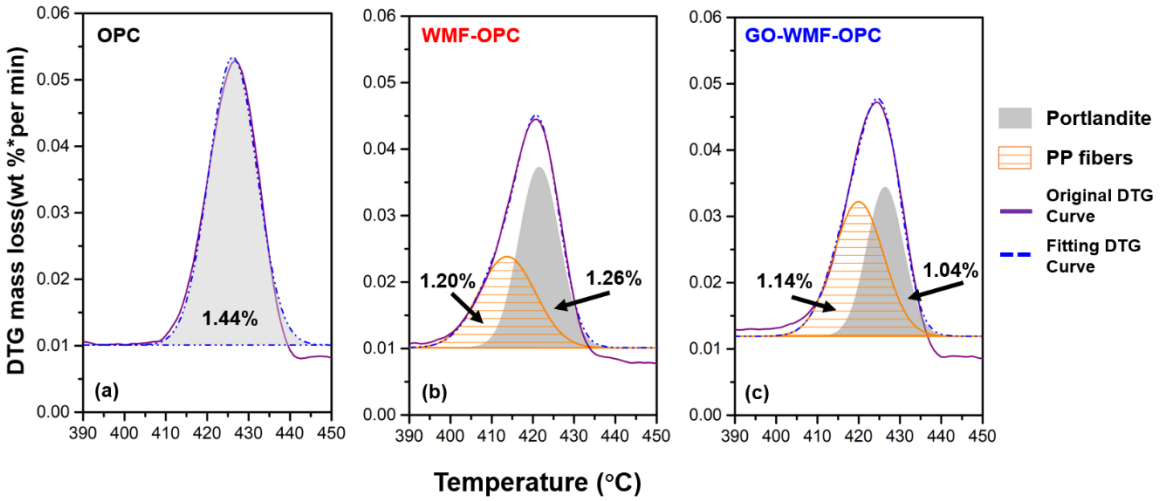

Figure 0.11. Gaussian peaks fitting for the 390°C~450°C DTG curves for pastes: (a) OPC, (b) WMF-OPC, and (c) GO-WMF-OPC, respectively.

The content of portlandite in the OPC, WMF-OPC, and GO-WMF-OPC pastes was 1.44 wt.%, 1.26 wt.%, and 1.04 wt.%, respectively. Less portlandite was detected in the GO-WMF-OPC, indicating that the admixed GO accelerated the hydration process and thus consumed more portlandite. The carbonate (650°C ~750°C) in GO-WMF-OPC was much less than other two samples, indicating the beneficial role of admixed GO in improving the carbonation resistance of cement paste, which was also reported by Long et al. and Mohammed et al. (Long et al., 2018; Mohammed et al., 2018) Note that the portlandite in WMF-OPC was less than in OPC sample, this is due to the conversion of portlandite to calcite (as revealed by the much higher content of carbonate in WMF-OPC). In other words, the admixed WMF induced defects into the cement paste and facilitated the reaction of portlandite with airborne CO_2.

4.4 Statistical Modeling for F/T damage and Service Life Prediction

Based on the F/T testing results which the failure scenario is specified by the ASTM C666, two-parameter Weibull models are fitted using maximum likelihood estimation (MLE) to discriminate the differences between the three designed mortars, and **Table 0.2** provides the paired shape and scale parameters for the fitted Weibull models. The testing results (p-values) of goodness-of-fit are provided in **Table 0.3.** The p-values of all tests were larger than 0.05, indicating that the null hypothesis (Ho) was not rejected; in other words, the observed data was consistent with the expected data and the Weibull distribution model was a good fit for the experimental data obtained in this study. Based on the fitted Weibull models, the probability density function (**Equation 4.1**), cumulative distribution function (i.e., unreliability, **Equation**

4.2), reliability function (**Equation 4.3**), and failure rate function (**Equation 4.4**) were developed (shown below), and the corresponding figures are provided in **Figure 0.12.**

Table 0.2. Paired shape and scale parameters for the three mortars.

Mortars	Shape Parameter	Scale Parameter
OPC	48.445	210.259
WMF-OPC	69.040	247.201
GO-WMF-OPC	54.942	257.422

Table 0.3. p-Values for Several Different Tests of the Goodness-of-Fit.

Tests	OPC	WMF	GO-WMF
Kolmogorov-Smirnov	0.2196	0.2215	0.2560
Cramer-von Mises	0.0570	00753	0.0887
Anderson-Darling statistic	0.3325	0.4558	0.5129

$$f(x\,|\,\gamma,\beta) = \frac{\gamma}{\beta^{\gamma}} x^{(\gamma-1)} exp\left\{-\left(\frac{x}{\beta}\right)^{\gamma}\right\} \tag{4.1}$$

$$F(x|\gamma,\beta) = 1 - exp\left\{-\left(\frac{x}{\beta}\right)^{\gamma}\right\} \tag{4.2}$$

$$R(x|\gamma,\beta) = 1 - F(x|\gamma,\beta) = exp\left\{-\left(\frac{x}{\beta}\right)^{\gamma}\right\} \tag{4.3}$$

$$\lambda(x|\gamma,\beta) = \frac{f(x|\gamma,\beta)}{R(x|\gamma,\beta)} = \frac{\gamma}{\beta^{\gamma}} x^{(\gamma-1)} \tag{4.4}$$

where β is the scale parameter that locates the Weibull distribution and γ is the shape parameter that mainly serves as an indicator for determining the failure scenario in reliability analysis.

As illustrated in **Figure 0.12a**, with the increase of scale parameter, the Weibull distribution moved further to the right, indicating more prominent capacity to resist frost damage. The shape parameters of all three models were larger than 1 and the distribution was right (negative)-skewed, suggesting the acceleratingly cumulative damage nature of the frost damage. In other words, the frost damage failure rate increases over time, which is confirmed by **Figure 0.12d**. As shown in **Figure 0.12b** and **Figure 0.12c**, when the unreliability (or reliability) reached up (or decreased down) to 50%, the OPC was expected to withstand only about 209 F/T cycles, whereas the WMF-OPC and GO-WMF-OPC could withstand about 246 and 256 F/T cycles, respectively.

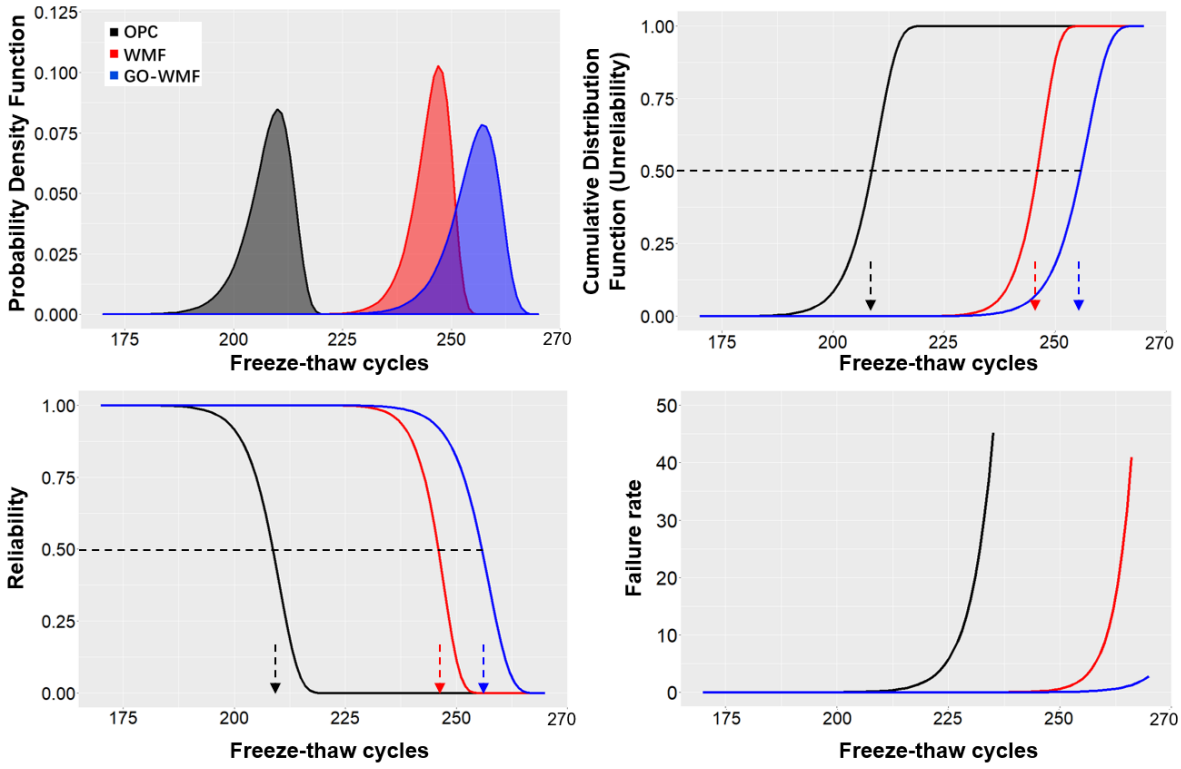

Figure 0.12. (a) Probability Density Function Plot; (b) Cumulative Distribution Function Plot (i.e., Unreliability vs. F/T Cycles Plot); (c) Reliability vs. F/T Cycles Plot; and (d) Failure Rate vs. F/T Cycles Plot of OPC, WMF, and GO-WMF Mortar Samples.

Service life prediction is an essential part of evaluating the long-term durability of cementitious composites under F/T conditions. In this study, three pavement systems located in Pullman, Washington, were modeled using OPC, WMF-OPC, and GO-WMF-OPC mortars.

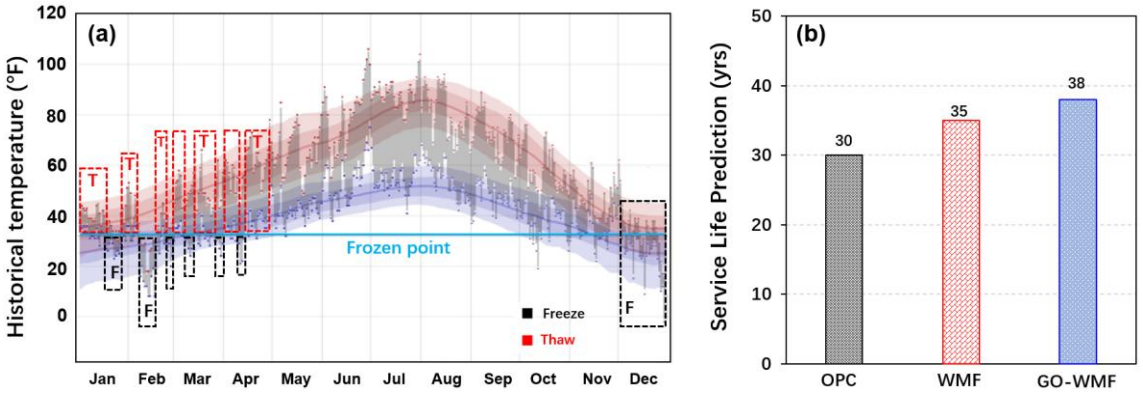

Figure 0.13. (a) Historical Temperature (°F) in Pullman, WA and (b) Predicted Service Life of OPC, WMF-OPC, and GO-WMF-OPC, Respectively.

Figure 0.13a presents the historical daily temperature profile of Pullman, illustrating the seasonal freeze–thaw behavior. Because freezing and thawing are dynamic processes, it is impractical to distinguish each cycle solely based on temperature fluctuations. To simplify this F/T modeling, the winter season was divided into approximately seven F/T cycles, as illustrated in **Figure 0.13a**. Based on the fitted Weibull distribution models, the predicted service lives of the three mortar types were estimated at 50 % reliability. The plain OPC mortar can withstand approximately 209 F/T cycles (equivalent to about 30 years of service), while the addition of WMF extended the endurance to about 246 F/T cycles ($\approx$ 35 years). The GO-WMF-OPC exhibited the best resistance to cyclic freezing and thawing, withstanding about 256 F/T cycles, corresponding to an estimated 38 years of service life (as illustrated in **Figure 0.13b**).

The enhanced durability of WMF- and GO-WMF-reinforced mortars reflects the fibers' ability to restrain microcrack propagation and mitigate freeze-induced damage. Furthermore, the GO modification strengthened the fiber–matrix interface and reduced moisture permeability, resulting in a more compact microstructure and longer predicted service life compared to both plain and unmodified fiber-reinforced mortars.

Chapter 5. Summary and Conclusions

This study investigated the potential of upcycling waste medical masks and textile fibers into high-performance cementitious composites through nanomaterial surface modification. The overall objective was to evaluate whether waste-derived polymer fibers, when combined with graphene oxide (GO) or nanoclay (NC), can serve as a cost-effective and sustainable alternative to commercial synthetic fibers for structural and infrastructure applications. The research included material processing, mechanical and durability testing, microstructural characterization, and probabilistic service life modeling. The major findings are summarized as follows:

1. The incorporation of a small amount of waste mask microfibers (0.1 vol.%) improved the tensile behavior of ordinary Portland cement (OPC) mortar without significantly affecting compressive strength. The fibers provided efficient crack-bridging and restrained microcrack propagation during loading and environmental exposure. Although a slight increase in porosity was observed, the mechanical benefits were evident, particularly in splitting tensile strength. These results demonstrate that properly processed waste mask fibers can be used as an effective reinforcing component in cementitious composites.

2. Surface treatment of fibers with trace amounts of GO or NC (0.02 wt.%) further enhanced the performance of the WMF-reinforced mortar. GO-modified fibers exhibited the highest improvement in tensile strength because of stronger interfacial bonding, enhanced load transfer, and improved crack-bridging capability. NC-modified fibers contributed to matrix densification and refined the pore structure, resulting in a measurable reduction in chloride permeability and improved resistance against environmental degradation. These findings highlight that both nanomaterials are effective modifiers, although their strengthening mechanisms differ.

3. The addition of nanomodified fibers significantly enhanced the durability of cementitious composites. GO-WMF and NC-WMF mortars exhibited lower chloride migration coefficients and higher electrical resistivity compared with plain and unmodified WMF mortars. NC-WMF displayed the greatest resistance to chloride ingress, indicating a denser and less connected pore network. Under freeze–thaw cycling, GO-WMF mortar retained higher mechanical strength and experienced slower degradation, confirming the benefits of improved interfacial adhesion. Under sulfate wetting–drying cycles, both WMF and GO-WMF mortars showed superior strength retention compared with OPC, indicating their potential for long-term use in aggressive environments.

4. Microstructural analyses using SEM, BSE, EDS, and TGA revealed that GO promoted the formation of dense calcium silicate hydrate and calcium-rich hydrates, reduced portlandite consumption, and improved the compactness of the interfacial transition zone. NC facilitated the formation of secondary gel phases and contributed to pore refinement. Although the two nanomaterials differ in their chemical reactivity, their overall influence on matrix densification and crack mitigation was consistent with the observed macroscopic improvements.

5. Probabilistic modeling using the Weibull distribution demonstrated that nanomodified fiber-reinforced mortars have extended service life under freeze–thaw conditions. The OPC mortar was estimated to withstand approximately 209 cycles, corresponding to about 30 years. The WMF-reinforced mortar extended this endurance to about 246 cycles, equivalent to 35 years. The GO-WMF mortar achieved the longest predicted service life of about 256 cycles, corresponding to 38 years. These results indicate that nanomodified waste-derived fibers can provide measurable long-term benefits for cold-climate infrastructure

In conclusion, research demonstrated that waste medical masks and textile fibers, when properly processed and modified with nanomaterials, can serve as effective reinforcing agents in OPC-based composites. The combined use of WMF and GO or NC significantly enhanced tensile performance, durability, and long-term resistance to environmental degradation. GO provided superior interfacial reinforcement and tensile improvement, while NC contributed to greater chloride resistance and matrix densification. The study provides a scientific basis for integrating recycled fibers and nanomaterials into sustainable cementitious composites and highlights a feasible pathway for converting pandemic-related waste into value-added construction materials.

This study highlighted several experimental considerations associated with nanomodified waste-derived fiber-reinforced cementitious composites. Variability in waste fiber geometry and dispersion introduced some scatter in mechanical test results, particularly for tensile properties. In addition, laboratory-based accelerated durability tests provided useful comparative insights but cannot fully represent long-term field exposure conditions. The effectiveness of graphene oxide and nanoclay surface modification was also sensitive to processing parameters such as dispersion quality and treatment sequence. These observations indicate that further optimization of fiber preprocessing, surface treatment protocols, and field-scale validation will be critical for ensuring consistent performance in practical infrastructure applications. Future research is recommended in the following areas:

1. Nanomaterial Hybridization: Investigate the combined effects of multiple nanomodifiers, alternative nanoclay types, and optimized dosages to further enhance interfacial bonding and durability.
2. Extended Durability Assessments: Conduct long-term testing under additional environmental stressors such as carbonation, alkali–silica reaction, ultraviolet exposure, and elevated temperature conditions.
3. Field-Scale Implementation: Perform pilot-scale construction trials to evaluate structural performance, workability, curing behavior, and degradation patterns under real environmental conditions.
4. Interfacial Mechanism Studies: Use advanced characterization tools to study the chemical and mechanical evolution of the fiber–matrix interface during hydration, loading, and cyclic damage processes.

5. Service Life and Multi-Hazard Modeling: Expand probabilistic modeling to include seismic loading, fire exposure, impact resistance, and combined environmental hazards.
6. Life Cycle and Economic Assessment: Quantify environmental benefits, carbon footprint reduction, and economic feasibility through life cycle assessment and cost–benefit analysis.

Chapter 6. Technology Transfer and Implementation

The findings of this study demonstrate strong potential for translating nanomodified waste-derived fiber-reinforced cementitious composites into practical infrastructure applications. The combination of improved tensile performance, enhanced durability, and extended service life positions this technology as a promising candidate for deployment in transportation-related construction and maintenance activities.

6.1 Potential Applications

Based on the observed mechanical and durability performance, the proposed materials are well suited for a range of transportation infrastructure applications where crack resistance and environmental durability are critical. Potential applications include cementitious overlays for bridge decks and pavements, patch repair mortars for localized distress remediation, and protective layers for concrete elements exposed to freeze–thaw cycling, chloride ingress, or sulfate attack. The enhanced tensile strength and crack-bridging capacity provided by the nanomodified waste fibers are particularly beneficial for thin-section applications, where conventional materials are prone to early-age cracking and durability-related degradation.

In addition, the compatibility of the proposed fiber system with conventional ordinary Portland cement mixtures suggests that implementation would not require substantial changes to existing mix design practices or construction workflows, thereby facilitating adoption in routine maintenance and rehabilitation projects.

6.2 Prospective Users and Stakeholders

Prospective users of this technology include state and local Department of Transportation (DOT) materials laboratories, which routinely evaluate and qualify new materials for infrastructure applications. The developed composites can be readily incorporated into laboratory-scale and pilot-scale testing programs for overlays, repair mortars, and durability-critical concrete elements.

Precast concrete producers also represent a key stakeholder group, as the enhanced durability and crack resistance of the proposed materials may improve product longevity and quality consistency in controlled manufacturing environments. Additional stakeholders include contractors specializing in pavement rehabilitation, bridge maintenance, and cold-climate infrastructure, as well as research institutions and university transportation centers seeking scalable solutions for waste utilization and durability enhancement.

6.3 Expected Cost and Life-Cycle Benefits

From a cost and sustainability perspective, the use of waste-derived polymer fibers offers a pathway to partially replace commercial synthetic fibers, which are typically produced from virgin petrochemical feedstocks. While detailed cost analysis was beyond the scope of this study, the use of waste-derived polymer fibers is expected to reduce material costs and provide long-term life-cycle benefits through enhanced durability and extended service life. More importantly, the demonstrated improvements in durability performance and predicted service life suggest meaningful life-cycle benefits. Reduced crack formation, lower chloride permeability, and

improved resistance to freeze–thaw and sulfate exposure are expected to decrease maintenance frequency, extend service intervals, and lower long-term rehabilitation costs for transportation infrastructure. These life-cycle advantages align closely with the mission of TriDurLE to enhance infrastructure durability and resilience through innovative and sustainable material solutions.

References

Amin, F., Javed, M.F., Ahmad, I., Asad, O., Khan, N., Khan, A.B., Ali, S., Abdullaev, S., Awwad, F.A., Ismail, E.A.A., 2024. Utilization of discarded face masks in combination with recycled concrete aggregate and silica fume for sustainable civil construction projects. Sci Rep 14, 449. https://doi.org/10.1038/s41598-023-50946-z

Chowdhury, I.Z., Mandal, S., Bazhaw-Hyscher, A., Rodriguez, L., England, A., Moody, M., Taylor, M., Hague, B., 2022. Perspectives of Textile Waste Management in the U.S. -A Review. Journal of Textile Science & Fashion Technology 9. https://doi.org/10.33552/JTSFT.2022.09.000716

Cui, J., Qi, M., Zhang, Z., Gao, S., Xu, N., Wang, X., Li, N., Chen, G., 2023. Disposal and resource utilization of waste masks: a review. Environ Sci Pollut Res 30, 19683–19704. https://doi.org/10.1007/s11356-023-25353-6

De-la-Torre, G.E., Dioses-Salinas, D.C., Pizarro-Ortega, C.I., Fernández-Severini, M.D., Forero-López, A.D., Dobaradaran, S., Selvasembian, R., 2023. Face mask structure, degradation, and interaction with marine biota: A review. Journal of Hazardous Materials Advances 10, 100326. https://doi.org/10.1016/j.hazadv.2023.100326

Famy, C., Scrivener, K.L., Atkinson, A., Brough, A.R., 2002. Effects of an early or a late heat treatment on the microstructure and composition of inner C-S-H products of Portland cement mortars. Cement and Concrete Research 32, 269–278. https://doi.org/10.1016/S0008-8846(01)00670-6

Friese, D., Scheurer, M., Hahn, L., Gries, T., Cherif, C., 2022. Textile reinforcement structures for concrete construction applications—a review. Journal of Composite Materials 56, 4041–4064. https://doi.org/10.1177/00219983221127181

Gao, B., Zhang, R., He, M., Sun, L., Wang, C., Liu, L., Zhao, L., Cui, H., Cao, A., 2016. Effect of a multiscale reinforcement by carbon fiber surface treatment with graphene oxide/carbon nanotubes on the mechanical properties of reinforced carbon/carbon composites. Composites Part A: Applied Science and Manufacturing 90, 433–440. https://doi.org/10.1016/j.compositesa.2016.08.012

Goldstein, J.I., Newbury, D.E., Michael, J.R., Ritchie, N.W.M., Scott, J.H.J., Joy, D.C., 2017. Scanning Electron Microscopy and X-Ray Microanalysis. Springer.

Gong, J., Li, Z., Zhang, R., Li, J., Shi, X., 2019. Synergistic Effects of Nano-Montmorillonite and Polyethylene Microfiber in Foamed Paste with High Volume Fly Ash Binder. Journal of Nanoscience and Nanotechnology 19, 4465–4473. https://doi.org/10.1166/jnn.2019.16353

Gong, J., Qian, Y., Xu, Z., Chen, C., Jin, Y., Zhang, J., Li, Z., Shi, X., 2024. Effect of graphene oxide on the properties of ternary limestone clay cement paste.

Nanotechnology Reviews 13. https://doi.org/10.1515/ntrev-2023-0222

He, J., Du, S., Yang, Z., Shi, X., 2018. Laboratory investigation of graphene oxide suspension as a surface sealer for cementitious mortars. Construction and Building Materials 162, 65–79. https://doi.org/10.1016/j.conbuildmat.2017.12.022

He, X., Shi, X., 2008. Chloride Permeability and Microstructure of Portland Cement Mortars Incorporating Nanomaterials. Transportation Research Record 2070, 13–21. https://doi.org/10.3141/2070-03

He, Y., Chen, Q., Wu, D., Zhou, M., Wang, T., Lu, C., Zhang, L., Liu, H., Liu, C., 2021. Effect of multiscale reinforcement by fiber surface treatment with polyvinyl alcohol/graphene oxide/oxidized carbon nanotubes on the mechanical properties of reinforced hybrid fiber composites. Composites Science and Technology 204, 108634. https://doi.org/10.1016/j.compscitech.2020.108634

Lei, Z., Li, Z., Zhang, X., Shi, X., 2021. Durability of CFRP-wrapped concrete in cold regions: A laboratory evaluation of montmorillonite nanoclay-modified siloxane epoxy adhesive. Construction and Building Materials 290, 123253. https://doi.org/10.1016/j.conbuildmat.2021.123253

Li, Z., Gong, J., Du, S., Wu, J., Li, J., Hoffman, D., Shi, X., 2017. Nano-montmorillonite modified foamed paste with a high volume fly ash binder. RSC Advances 7, 9803–9812. https://doi.org/10.1039/C6RA26968K

Li, Z., Shi, X., 2020. Graphene oxide modified, clinker-free cementitious paste with principally alkali-activated fly ash. Fuel 269, 117418. https://doi.org/10.1016/j.fuel.2020.117418

Li, Z., Zhang, Z., Fei, M., Shi, X., 2022. Upcycling waste mask PP microfibers in portland cement paste: Surface treatment by graphene oxide. Materials Letters 318, 132238. https://doi.org/10.1016/j.matlet.2022.132238

Li, Z., Zhang, Z., He, J., Shi, X., 2024. Graphene Oxide–Pretreated Waste Medical Mask Microfiber-Reinforced Cement Composites: Frost Damage Modeling and Chloride Migration. Journal of Materials in Civil Engineering 36, 04023506. https://doi.org/10.1061/JMCEE7.MTENG-16371

Liang, H., Ji, Y., Ge, W., Wu, J., Song, N., Yin, Z., Chai, C., 2022. Release kinetics of microplastics from disposable face masks into the aqueous environment. Science of The Total Environment 816, 151650. https://doi.org/10.1016/j.scitotenv.2021.151650

Liu, J., Jia, Y., Wang, J., 2019. Calculation of chloride ion diffusion in glass and polypropylene fiber-reinforced concrete. Construction and Building Materials 215, 875–885. https://doi.org/10.1016/j.conbuildmat.2019.04.246

Long, W.-J., Gu, Y., Xing, F., Khayat, K.H., 2018. Microstructure development

and mechanism of hardened cement paste incorporating graphene oxide during carbonation. Cement and Concrete Composites 94, 72–84. https://doi.org/10.1016/j.cemconcomp.2018.08.016

Lu, S., Liu, J., Tian, Z., Lu, Y., Liang, G., Zhang, L., Bian, H., 2025. Deterioration mechanisms and strength prediction of hybrid fiber-reinforced concrete under coupled sulfate attack and dry-wet cycles. Construction and Building Materials 493, 143243. https://doi.org/10.1016/j.conbuildmat.2025.143243

Lyu, L., Bagchi, M., Ng, K.T.W., Markoglou, N., Chowdhury, R., An, C., Chen, Z., Yang, X., 2024. The degradation of polylactic acid face mask components in different environments. Journal of Environmental Management 370, 122731. https://doi.org/10.1016/j.jenvman.2024.122731

Lyu, L., Wang, Z., Bagchi, M., Ye, Z., Soliman, A., Bagchi, A., Markoglou, N., Yin, J., An, C., Yang, X., Bi, H., Cai, M., 2023. An investigation into the aging of disposable face masks in landfill leachate. Journal of Hazardous Materials 446, 130671. https://doi.org/10.1016/j.jhazmat.2022.130671

Mansi, A., Sor, N.H., Hilal, N., Qaidi, S.M.A., 2022. The Impact of Nano Clay on Normal and High-Performance Concrete Characteristics: A Review. IOP Conf. Ser.: Earth Environ. Sci. 961, 012085. https://doi.org/10.1088/1755-1315/961/1/012085

Moazzem, S., Wang, L., Daver, F., Crossin, E., 2021. Environmental impact of discarded apparel landfilling and recycling. Resources, Conservation and Recycling 166, 105338. https://doi.org/10.1016/j.resconrec.2020.105338

Mohammed, A., Sanjayan, J.G., Nazari, A., Al-Saadi, N.T.K., 2018. The role of graphene oxide in limited long-term carbonation of cement-based matrix. Construction and Building Materials 168, 858–866. https://doi.org/10.1016/j.conbuildmat.2018.02.082

Ray, S.S., Lee, H.K., Huyen, D.T.T., Chen, S.-S., Kwon, Y.-N., 2022. Microplastics waste in environment: A perspective on recycling issues from PPE kits and face masks during the COVID-19 pandemic. Environmental Technology & Innovation 26, 102290. https://doi.org/10.1016/j.eti.2022.102290

Skrzyniarz, M., Sajdak, M., Zajemska, M., Iwaszko, J., Biniek-Poskart, A., Skibiński, A., Morel, S., Niegodajew, P., 2022. Plastic Waste Management towards Energy Recovery during the COVID-19 Pandemic: The Example of Protective Face Mask Pyrolysis. Energies 15, 2629. https://doi.org/10.3390/en15072629

Vespa, M., Wieland, E., Dähn, R., Grolimund, D., Scheidegger, A.M., 2007. Determination of the elemental distribution and chemical speciation in highly heterogeneous cementitious materials using synchrotron-based micro-spectroscopic techniques. Cement and Concrete Research 37, 1473–1482. https://doi.org/10.1016/j.cemconres.2007.08.007

Wang, Y., Zhang, S., Niu, D., Fu, Q., 2022. Quantitative evaluation of the characteristics of air voids and their relationship with the permeability and salt freeze–thaw resistance of hybrid steel-polypropylene fiber–reinforced concrete composites. Cement and Concrete Composites 125, 104292. https://doi.org/10.1016/j.cemconcomp.2021.104292

Wang, Ying, Wang, Yingying, Li, Y., Hu, X., 2025. Recycling mask waste into fiber-reinforced concrete: tailoring thermal and humidity response via pore structure optimization and life cycle assessment. Thermal Science and Engineering Progress 65, 103903. https://doi.org/10.1016/j.tsep.2025.103903

Williams Portal, N., Lundgren, K., Wallbaum, H., Malaga, K., 2015. Sustainable Potential of Textile-Reinforced Concrete. Journal of Materials in Civil Engineering 27, 04014207. https://doi.org/10.1061/(ASCE)MT.1943-5533.0001160

Xu, G., Du, S., He, J., Shi, X., 2019. The role of admixed graphene oxide in a cement hydration system. Carbon 148, 141–150. https://doi.org/10.1016/j.carbon.2019.03.072

Xu, G., Zhong, J., Shi, X., 2018. Influence of graphene oxide in a chemically activated fly ash. Fuel 226, 644–657. https://doi.org/10.1016/j.fuel.2018.04.033

Yao, X., Shamsaei, E., Chen, S., Zhang, Q.H., de Souza, F.B., Sagoe-Crentsil, K., Duan, W., 2019. Graphene oxide-coated Poly(vinyl alcohol) fibers for enhanced fiber-reinforced cementitious composites. Composites Part B: Engineering 174, 107010. https://doi.org/10.1016/j.compositesb.2019.107010

Zhang, F., Li, X., Wang, D., 2024. Mechanical behavior of self-compacting recycled concrete reinforced with recycled disposable medical mask fiber. Construction and Building Materials 429, 136314. https://doi.org/10.1016/j.conbuildmat.2024.136314

Zhang, Z., Li, Z., He, J., Qian, S., Shi, X., 2024. Recycled mask polypropylene microfibers benefit tensile properties and prevent thermally induced spalling of high-strength engineered cementitious composite (HS-ECC). Journal of Cleaner Production 457, 142476. https://doi.org/10.1016/j.jclepro.2024.142476